Research Article

Algae 2023, 38(1): 1-22
https://doi.org/10.4490/algae.2023.38.3.9
Open Access

The description of *Haematococcus privus* sp. nov. (Chlorophyceae, Chlamydomonadales) from North America

Mark A. Buchheim*, Ashley Silver, Haley Johnson, Richard Portman and Matthew B. Toomey

Department of Biological Science, The University of Tulsa, 800 South Tucker Dr., Tulsa, OK 74104, USA

An enormous body of research is focused on finding ways to commercialize carotenoids produced by the unicellular green alga, *Haematococcus*, often without the benefit of a sound phylogenetic assessment. Evidence of cryptic diversity in the genus means that comparing results of pigment studies may be confounded by the absence of a phylogenetic framework. Moreover, previous work has identified unnamed strains that are likely candidates for species status. We reconstructed the phylogeny of an expanded sampling of *Haematococcus* isolates utilizing data from nuclear ribosomal markers (18S rRNA gene, 26S rRNA gene, internal transcribed spacer [ITS]-1, 5.8S rRNA gene, and ITS-2) and the *rbc*L gene. In addition, we gathered morphological, ultrastructural and pigment data from key isolates of *Haematococcus*. Our expanded data and taxon sampling support the concept of a new species, *H. privus*, found exclusively in North America. Despite overlap in numerous morphological traits, results indicate that ratios of protoplast length to width and akinete diameter may be useful for discriminating *Haematococcus* lineages. High growth rate and robust astaxanthin yield indicate that *H. rubicundus* (SAG 34-1c) is worthy of additional scrutiny as a pigment source. With the description of *H. privus*, the evidence supports the existence of at least five, species-level lineages in the genus. Our phylogenetic assessment provides the tools to frame future pigment investigations of *Haematococcus* in an updated evolutionary context. In addition, our investigation highlighted open questions regarding polyploidy and sexuality in *Haematococcus* which demonstrate that much remains to be discovered about this green flagellate.

Keywords: astaxanthin; *Haematococcus privus*; HPLC; *rbc*L; rRNA

INTRODUCTION

Recent molecular phylogenetic evidence led to major taxonomic and systematic revision that stripped the green algal genus, *Haematococcus* Flotow, of all but one species, (*H. lacustris* Flotow) (Buchheim et al. 2013). In addition, a number of investigations revealed multiple lineages among taxa originally ascribed to that single species, *H. lacustris* (Girod-Chantrans) Rostafinski (Buchheim et al. 2013, Allewaert et al. 2015, Chekanov et al. 2020). Buchheim et al. (2013) originally identified five lineages that were referred to as Pluvialis A–E. *Haematococcus pluvialis* is now regarded as a synonym of *H. lacustris* (Nakada and Ota 2016), but at the time of our publication the consensus was that *H. pluvialis* was the legitimate species name, hence, the reference to "Pluvialis" isolates in Buchheim et al. (2013). Members from two of these lineages (Pluvialis C [minus the SAG 34-1f isolate] and Pluvialis E) are now recognized as new species, *H. rubicundus* Allewaert et Vanormelingen and *H. rubens* Allewaert et Vanormel-

Received September 17, 2022, **Accepted** March 9, 2023
***Corresponding Author**
E-mail: mark-buchheim@utulsa.edu
Tel: +1-918-631-3833

ingen, respectively (Allewaert et al. 2015). In addition, Allewaert et al. (2015) affirmed the distinctiveness of the Pluvialis D (SAG 44.96) lineage but persuasively argued that SAG 34-1f should also be accorded status as a distinct lineage. At present, neither of these two lineages has been described as new species. Mazumdar et al. (2018) revealed yet a fourth new species, *H. alpinus* Mazumdar et Gopalakrishnan, that was isolated from a high elevation habitat in New Zealand. Chekanov et al. (2020) did not introduce a new species but their data revealed the existence of a distinct clade of polar isolates of *H. lacustris*.

Allewaert et al. (2015), who focused exclusively on European isolates, noted that allies of Pluvialis B (*sensu* Buchheim et al. 2013) were not encountered in their collections or surveys. Neither Mazumdar et al. (2018) nor Chekanov et al. (2020) reported any strains that could be ascribed to the Pluvialis B lineage in their survey of alpine New Zealand and the White Sea polar region, respectively. Lastly, work that focused on collecting and identifying *Haematococcus* isolates in South America (González et al. 2009, Gómez et al. 2016) have similarly failed to yield isolates that can be attributed to the "Pluvialis B" lineage in *Haematococcus*. In short, *Haematococcus* is now comprised of four species coupled with evidence of the existence of three additional lineages. Although Allewaert et al. (2015) presented evidence of distinct morphological and physiological traits, they also noted that much variability overlapped across lineages. Chelebieva et al. (2018) recorded developmental and biochemical variability among three isolates of *H. lacustris* (IMBR-1, IMBR-2, and IMBR-3) despite near molecular phylogenetic identity among the isolates. Moreover, all of the isolates and species produce an akinete stage that accumulates astaxanthin. Thus, from a practical standpoint, much of the morphological and physiological variation across the genus can be regarded as cryptic.

As noted above, just a handful of scientists have focused on expanding our understanding of *Haematococcus* diversity. In contrast, the overwhelming majority of effort and resources directed towards the study of *Haematococcus*—more than 100 citations since 2021 (Google Scholar search on May 19, 2022)—is being expended to optimize induction, extraction, and commercialization of valuable carotenoids. Unfortunately, it appears that at least some of this applied research is being done in the absence of an understanding of the phylogenetic diversity that was revealed in the last decade. Review articles on pigment analysis and optimization (e.g., Ahirwar et al. 2021, Oslan et al. 2021, Kim et al. 2022, Mota et al. 2022) summarize studies of *H. lacustris* (as *H. pluvialis* in most cases) exclusively, either ignoring the recent revelations regarding *Haematococcus* diversity (Buchheim et al. 2013, Allewaert et al. 2015, Mazumdar et al. 2018, Chekanov et al. 2020) or accepting suspect identifications reported in the myriad publications that serve as the basis for the review articles. For example, a number of pigment investigations relied solely on analyses of the 18S rRNA gene for species identification (e.g., Wang et al. 2019, Guo et al. 2021, Yu et al. 2021, Karuppan et al. 2022). Our research has shown that the highly-conserved 18S rRNA gene sequences fail to unambiguously resolve most strains that have been identified as distinct by other markers (e.g., internal transcribed spacer [ITS]-2). Lastly, some publications do not present any phylogenetic evidence validating their application of the name, *H. lacustris* or *H. pluvialis*, to the strain(s) used in the investigation (e.g., Ashokkumar et al. 2021, Du et al. 2021, Fang et al. 2022). A cursory survey of the literature indicates that at least seven strains (GXU-A23, H_2, HP5, IBCE H-17, LUGU, NBU489, and ZY-18) used in a number of investigations have not been phylogenetically validated as *H. lacustris*. While this nomenclatural issue does not impugn the experimental design of an investigation, it does confound our ability to make comparative assessments of the experimental results among research groups and over time.

Our intent with this publication is to provide a substantive update to an assessment of phylogenetic and taxonomic diversity in *Haematococcus* that can inform both basic and applied research programs. To that end, the focus of this investigation is a formal description, as *Haematococcus privus* sp. nov., of the "Pluvialis B" organisms (*sensu* Buchheim et al. 2013) that have been collected exclusively from North America. Although the results from molecular phylogenetic analysis provide the bulk of support for describing a new species of *Haematococcus*, some morphological traits (e.g., akinete diameter) and pigment data (e.g., astaxanthin yield) may help to set this lineage apart from other species of *Haematococcus*. We also offer additional insight into the importance of several intriguing observations regarding the basic biology of *Haematococcus* that would be relevant for both basic and applied research.

MATERIALS AND METHODS

All *Haematococcus* taxa included in various analyses undertaken in this investigation are presented in Supplementary Table S1. Isolates targeted for microscopy are

identified and GenBank accession numbers are listed for taxa included in the six different molecular phylogenetic analyses (18S rRNA, 26S rRNA, *rbc*L, ITS-1 rRNA, 5.8S rRNA, ITS-2 rRNA) (Supplementary Table S1).

Light microscopy

Cells for light microscopy (differential interference contrast [DIC] and phase contrast [PC] optics) were grown in glass tube culture (5 mL) or flask culture (50 mL) using liquid *Volvox* medium (McCracken et al. 1980). Cells were either viewed as living specimens or fixed in 2% (v : v) glutaraldehyde in growth medium contained in 1.5 mL Eppendorf tubes. All cells were photographed at 40× (DIC or PC) using an AmScope MU1000 camera and software (AmScope x64, 4.11.1786420201020; Amscope, Irvine, CA, USA) attached to an Olympus BH2 chassis (Olympus America, Center Valley, PA, USA) equipped with a halogen source (12 V, 100 W, 3200K color temperature). Recorded images were measured using the tools that accompany the AmScope x64 software application. Eight different cell dimensions (Supplementary Table S2) or attributes were recorded for 43 randomly selected motile (flagellated) cells for three *H. privus* isolates (HP136, HP137, and HP138), two *H. lacustris* isolates (NIES-144 and SAG 49.94), one isolate of *H. rubicundus* (SAG 34-1c) and one isolate of *H. rubens* (SAG 34-1h). Using data collected by Allewaert et al. (2015) as a guide, ratios of cell length to width and protoplast length to width were calculated for motile cells from all isolates in the comparison. Motile cell length was measured from the cell wall apex at the midpoint between the emerging flagella to the posterior-most point on the outer cell wall boundary. Motile cell diameter was measured outer cell wall boundary to outer cell wall boundary at the broadest point and normal to the line of cell length. Protoplast length of motile cells was measured from the cell apex where flagella emerge from the protoplast to the posterior-most point of the protoplast. Protoplast diameter of motile cells was measured protoplast boundary to protoplast boundary at the broadest point and normal to the line of protoplast length. Cell diameter (wall to wall) was recorded for 43, randomly-selected akinetes for the same set of *Haematococcus* isolates.

Statistical analysis

In advance of statistical analysis of measurements data, the shape of the distribution was evaluated using the Shapiro Wilk test (Shapiro Wilk test calculator, Statistics Kingdom 2017) to test for normality. Since a few sets of data failed the Shapiro Wilk test, all comparisons were completed using non-parametric tests using online tools for the Wilcoxon Signed-Ranks test (Wilcoxon Signed-Ranks test calculator, Statistics Kingdom 2017) and the Mann-Whitney U test (Mann Whitney U test calculator, Statistics Kingdom 2017). Parametric statistical analyses (single factor analysis of variance [ANOVA]) were conducted using the tools in Excel. Standard error of the mean was calculated manually in Microsoft Excel for 365 (v. 2210 Build 16.0.15726.20188; Microsoft Corp., Redmond, WA, USA). All graphs were generated in Excel. Alpha was set to 0.05 for all relevant analyses.

Transmission electron microscopy

Motile cells of the HP136 isolate were harvested by centrifugation, fixed, embedded, and thin-sectioned for transmission electron microscopy (TEM) analysis using the protocol of Pegg et al. (2015). All images were digitally recorded using a Hitachi H7000 transmission electron microscope operated at an accelerating voltage of 75 kV (Hitachi High Technologies America, Schaumburg, IL, USA).

Molecular phylogeny

Extraction of nucleic acid, amplification of target DNA, and DNA sequencing was conducted as described previously (Buchheim et al. 2001, 2005, 2010, 2013). All sequences were assembled and edited using Sequencher vs 4.9 (Gene Codes, Ann Arbor, MI, USA). Edited sequences were imported into alignments where indels and substitutions were checked for accuracy. All sets of sequences except *rbc*L, ITS-2, and 5.8S rRNA were initially aligned using MUSCLE (Edgar 2004) as implemented in Mesquite 3.61 (Maddison and Maddison 2019). The ITS-2 data were initially aligned with the aid of secondary structure models (see below). The *rbc*L and 5.8S rRNA data were aligned manually. Manual alignment adjustments were completed using Mesquite. All data sets were analyzed using neighbor-joining (NJ), maximum likelihood (ML) as implemented in PAUP* (Swofford 2003) and Bayesian inference (BI) as implemented in MrBayes 3.2.7 (Ronquist et al. 2012). Models of nucleotide substitution were selected by Akaike best fit analysis as implemented in PAUP* (Swofford 2003). Bootstrap analysis (Felsenstein 1985) was used to identify relative support for nodes of the trees generated by ML and NJ analyses. Bootstrap proportions and posterior probabilities were mapped to

the corresponding nodes for each tree. All within and between group p-distances were calculated using MEGA7 (Kumar et al. 2016).

18S rRNA. The aligned 18S rRNA data set was comprised of 1,727 sites. A total of 83 taxa representing a broad sampling of chlamydomonadalean taxa were included in the analysis of 18S rRNA data. A list of the 16 *Haematococcus* and *Ettlia* Komárek taxa included in the analyses of the 18S data and their provenances are presented in Supplementary Table S1. All trees were rooted with data from sphaeroplealean taxa (i.e., part of a sister group to the Chlamydomonadales).

26S rRNA. The aligned 26S rRNA data set was comprised of 2,037 sites. A total of 20 taxa comprising select members of the Chlorogonia clade (*sensu* Nakada et al. 2008) were included in the analyses. A list of the 15 *Haematococcus* and *Ettlia* taxa included in the analyses of the 26S data and their provenances are presented in Supplementary Table S1. All trees were rooted with data from *Chlamydomonas applanata* Pringsheim (Polytominia *sensu* Nakada et al. 2008).

***rbc*L.** The aligned *rbc*L data set was comprised of 1,125 sites for all but three sequences. Despite using primer pairs that generally yielded a product comprising more than 1 kb of the *rbc*L gene, our amplification protocols produced much smaller polymerase chain reaction (PCR) products for *H. privus* isolates (<700 bases using ChlorRbclF and ChlorRbclR) (Kim et al. 2015) and for *Ettlia carotinosa* Komárek (<500 bases; rbcL1 and rbcL4) (Nozaki et al. 1995). Partial overlapping sequences from two strains of *H. privus* (HP137 and HP138) were combined into a single composite taxon for analysis of the *rbc*L data. A total of 26 taxa comprising select members of the Chlorogonia clade (*sensu* Nakada et al. 2008) was included in all analyses. A list of the 17 *Haematococcus* and *Ettlia* taxa included in the analyses of the *rbc*L data and their provenances are presented in Supplementary Table S1. All trees were rooted with data from *C. applanata* (Polytominia *sensu* Nakada et al. 2008).

ITS-1. The aligned ITS-1 data set was comprised of 449 sites. A total of 34 sequences representing principally *Haematococcus* and *Ettlia* taxa were included in all ITS-1 analyses. A list of the 31 *Haematococcus* and *Ettlia* taxa included in the analyses of the ITS-1 data and their provenances are presented in Supplementary Table S1. The trees were rooted with data from *C. applanata* (Polytominia *sensu* Nakada et al. 2008).

5.8S rRNA. The aligned 5.8S rRNA data set was comprised of 155 sites. A total of 33 sequences representing principally *Haematococcus* and *Ettlia* taxa were included in all 5.8S rRNA analyses. A list of the 30 *Haematococcus* and *Ettlia* taxa included in the analyses of the ITS-1 data and their provenances are presented in Supplementary Table S1. All trees were rooted with data from *C. applanata* (Polytominia *sensu* Nakada et al. 2008).

ITS-2. The aligned ITS-2 data set was comprised of 255 sites. Raw primary sequence data containing the ITS2 gene were annotated by comparison with other fully-annotated ITS2 sequences from existing alignments (Buchheim et al. 2013, Pegg et al. 2015). Secondary structure models for a number of ITS2 gene sequences from *Haematococcus* isolates (Buchheim et al. 2013, Pegg et al. 2015) were used as templates for homology modeling of secondary structure as implemented in the ITS2 Database V (Ankenbrand et al. 2015). Secondary structures for new ITS2 sequences from isolates of *Haematococcus* that cluster with existing species were modeled using corresponding templates (*H. lacustris* SAG 34-1b, *H. rubens* SAG 34-1h, and *H. rubicundus* SAG 34-1m). Homology modeling identified the template for *Haematococcus* sp. SAG 34-1f as producing the highest helix transfer percentages for the ITS2 from new *Haematococcus* (*H. privus*) isolates that form a monophyletic group based on preliminary analyses. Homology modeling identified the templates for *Haematococcus* sp. SAG 34-1f and *H. rubicundus* SAG 34-1m as producing the highest helix transfer percentages for the ITS2 from *H. alpinus*. Unfortunately, some short sequences plus the presence of ambiguous base calls reflecting either sequencing error or intragenomic variability (Alanagreh et al. 2017) in a number of ITS-2 sequences confounded our ability to obtain reliable sequence-structure alignments. Consequently, we used a secondary-structure-guided ITS-2 alignment in a final round of manual sequence alignment. All trees were rooted with data from *C. applanata* (Polytominia *sensu* Nakada et al. 2008).

Induction of carotenoid accumulation

To examine carotenoid content, select strains of *Haematococcus* (*H. lacustris* [NIES-144], *H. rubicundus* [SAG 34-1c], *H. rubens* [SAG 34-1h], *H. privus* [HP136], and *H. privus* [HP137]) were first grown in *Volvox* medium to bring all cells to the motile stage. Cell densities were measured using a Countess III automated cell counter (Invitrogen, Waltham, MA, USA) with disposable counting cells. Carotenoid induction experiments were initiated with three replicates for each strain where a total of 9,180 cells per mL, or approximately 45,900 motile cells were inoculated into 5 mL of Volvox medium (minus glycero-

phosphate) and grown in high light (714 μmol photons m^{-2} s^{-1}) using a MAXSISUN MF1000 Grow Light, 100 Watt LED panel on a 12 h : 12 h LD cycle at 23°C for 14 days.

Carotenoid analysis

Carotenoids were extracted from each replicate sample at the end of 14 days. Cell densities for each replicate were measured using a Countess III automated cell counter (Invitrogen) with disposable counting cells. Pelleted cells for each replicate were resuspended in a 0.9% NaCl solution (500 μL) with absolute ethanol (200 μL). Cells were subjected to three rounds of grinding with 0.1 g of 2 mm diameter zirconium beads for 180 s at 4,000 Hz using a Beadbug homogenizer (Benchmark Scientific, Sayreville, NJ, USA). A total of 500 μL of a 1 : 1 (v : v) solution of hexane : methyl *tertiary*-butyl ether (MTBE) was added to the extract and subjected to one round of homogenization (180 s at 4,000 Hz). The solvent layer was recovered after centrifugation (12,000 rpm for 3 min) in a 9 mL screw cap tube and following each round of homogenization. A fresh 500 μL of the 1 : 1 solution of hexane : MTBE was added to the homogenate tube and the process repeated two more times. The solvent layer from the three rounds of extraction was dried under a stream of nitrogen gas and stored at -80° under nitrogen gas. All raw extracts were prepared for analysis by mild saponification with 1,000 μL of 0.02 M NaOH in methanol for four hours in the dark in a 9 mL glass tube capped under nitrogen. The saponified extract was then re-extracted by adding 1,000 μL of saturated NaCl solution, followed by 2,000 μL of ultrapure water and then 2,000 μL of hexane : MTBE (1 : 1) and mixing by vortex at each step. This solution was then centrifuged for 5 min at 2,500 rpm using an Eppendorf 5417C benchtop centrifuge (Eppendorf Manufacturing Corp., Enfield, CT, USA). The solvent layer was recovered to 2 mL screw cap tubes, dried under nitrogen and stored at -80° under nitrogen.

High-performance liquid chromatography (HPLC) was used to identify and quantify the carotenoid content in the samples. The dried and saponified extracts for each replicate sample were resuspended in 500 μL of methanol : acetonitrile (1 : 1) by heating to 50°C for up to 2 h and vortexing intermittently to dissolve any remaining pigment. A total of 50 μL of each sample was then injected into an Agilent 1200 series HPLC (Agilent, Santa Clara, CA, USA) and separated by reverse-phase chromatography on a C30 column (5.0 μm, 4.6 mm × 250 mm, YMC, CT99S05-2546WT) heated to 30°C. The mobile phase was pumped at a constant rate of 1.2 mL min^{-1} and consisted of a gradient of acetonitrile : methanol : dichloromethane (44 : 44 : 12) (v : v : v) from 0 to 11 min, ramping up to acetonitrile : methanol : dichloromethane (35 : 35 : 30) from 11–21 minutes followed by isocratic conditions through 30 min, and then a return to initial conditions in minutes 30–33. The samples were monitored with a UV-Vis diode array detector at 445 and 480 nm. Astaxanthin was identified and quantified by comparison to an authentic external standard (gift of DSM Inc.).

RESULTS

Light and electron microscopy

Results from morphometric analysis of a suite of traits are presented in Supplementary Table S2. In addition to data for *Haematococcus* sp. (Pluvialis 5 lineage), comparison data from two strains of *H. lacustris*, one strain of *H. rubens*, one strain of *H. rubicundus* and the published data *for H. rubens* and *H. rubicundus* are included in Supplementary Table S2.

Motile cell shape for all three isolates of *H. privus* studied varied from ovate (Fig. 1A–E) in younger cells to nearly spherical in older cells or sporangia (Fig. 1F). Motile cell length ranged from 19.2 to 42.5 μm and motile cell width ranged from 15.8 to 36.9 μm. All three strains produced at least some motile cells bearing a wall papillum (Fig. 1D) but the presence of a wall papillum varied between strains. The cell wall of motile cells is thin (Figs 1A–D, 2D, 2F, 3A, B & E) and is separated from the protoplast by periplasmic spaces generally bounded by thin, cytoplasmic strands (see below). Save for the cytoplasmic strands, light microscopy does not reveal evidence of substance in the periplasmic space, but thin sections suggest the presence of a quasi-fibrous or granular material (Figs 2D, F & 3A–E). Protoplast length in motile cells ranged from 19.1 to 31.8 μm and protoplast width ranged from 11.4 to 28.0 μm. Protoplast shape in motile cells varied from shallowly lobate (Fig. 1A) to ovate / obtuse (Fig. 1B & D) to elliptic (Fig. 1C, E & F). Most cells that were observed bore a plasma papillum (i.e., acuminate end) at the cell apex where the flagella are inserted and the flagellar collars meet the protoplast (Fig. 1B & D). The chloroplast generally did not extend into the plasma papillum. Cells lacking a wall papillum were generally associated with larger and more spherical protoplasts (e.g., Fig. 1C). Cytoplasmic strands traversing the periplasmic space were generally present (Figs 1A, B, D, 2D & 3B), often branched near the cell wall boundary (Fig. 1A, arrows). When cytoplasmic strands

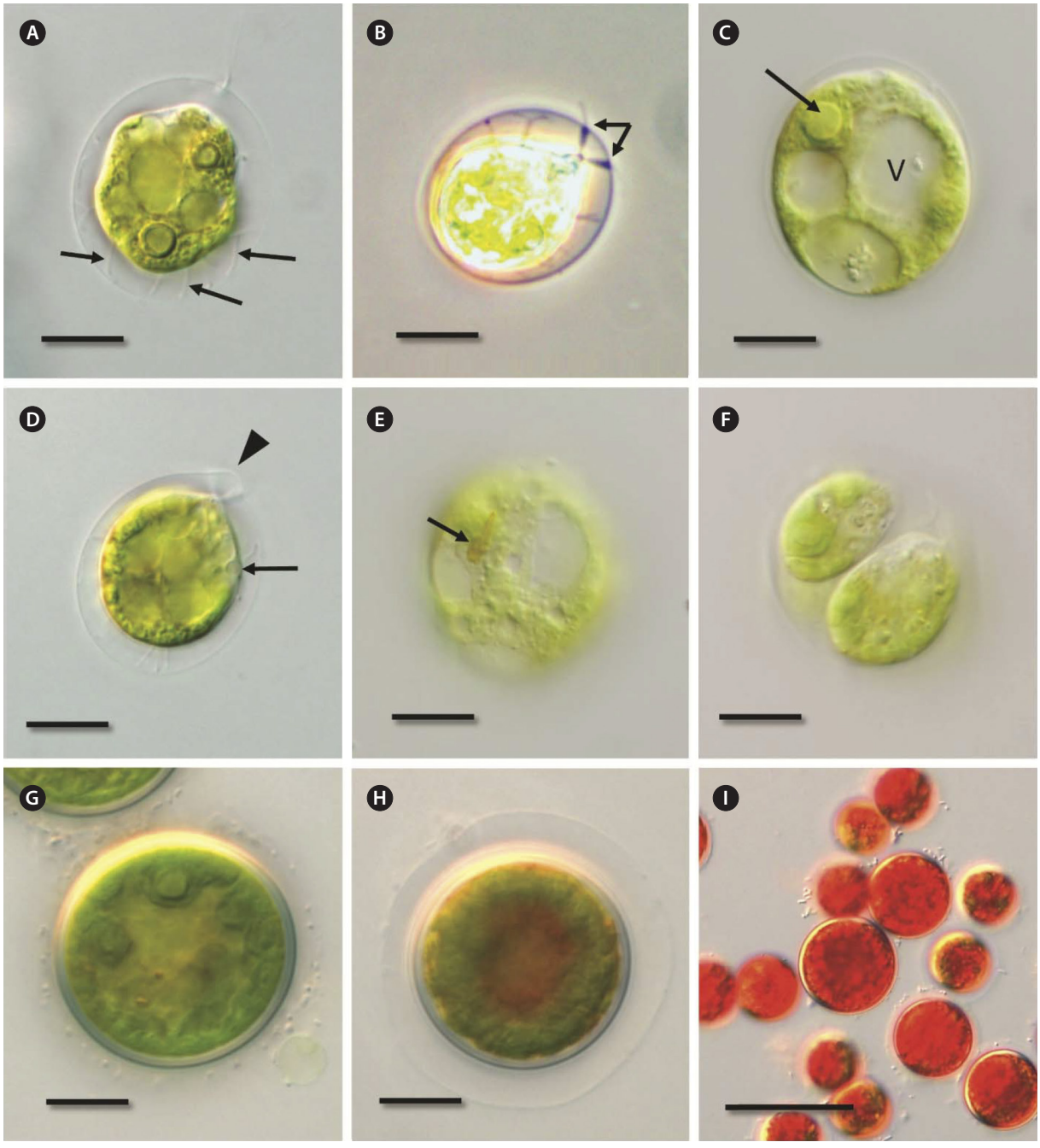

Fig. 1. Light microscope images for a range of stages for *Haematococcus privus*. (A) Flagellate stage with periplasmic space bearing a number of cytoplasmic strands (arrows; differential interference contrast [DIC] optics). (B) Flagellate stage bearing branched, cytoplasmic strands and flagellar collars (arrow; phase contrast optics). (C) Flagellate stage illustrating vacuoles (V) and pyrenoid (arrow; DIC optics). (D) Flagellate stage illustrating apical cell wall prominence (arrowhead) and contractile vacuole (arrow; DIC optics). (E) Flagellate stage illustrating stigma (arrow; DIC optics). (F) Sporangial cell illustrating daughter cells from asexual reproduction (DIC optics). (G) Palmella stage (DIC optics). (H) Early akinete stage (DIC optics). (I) Akinetes (DIC optics). Scale bars represent: A–H, 10 μm; I, 50 μm.

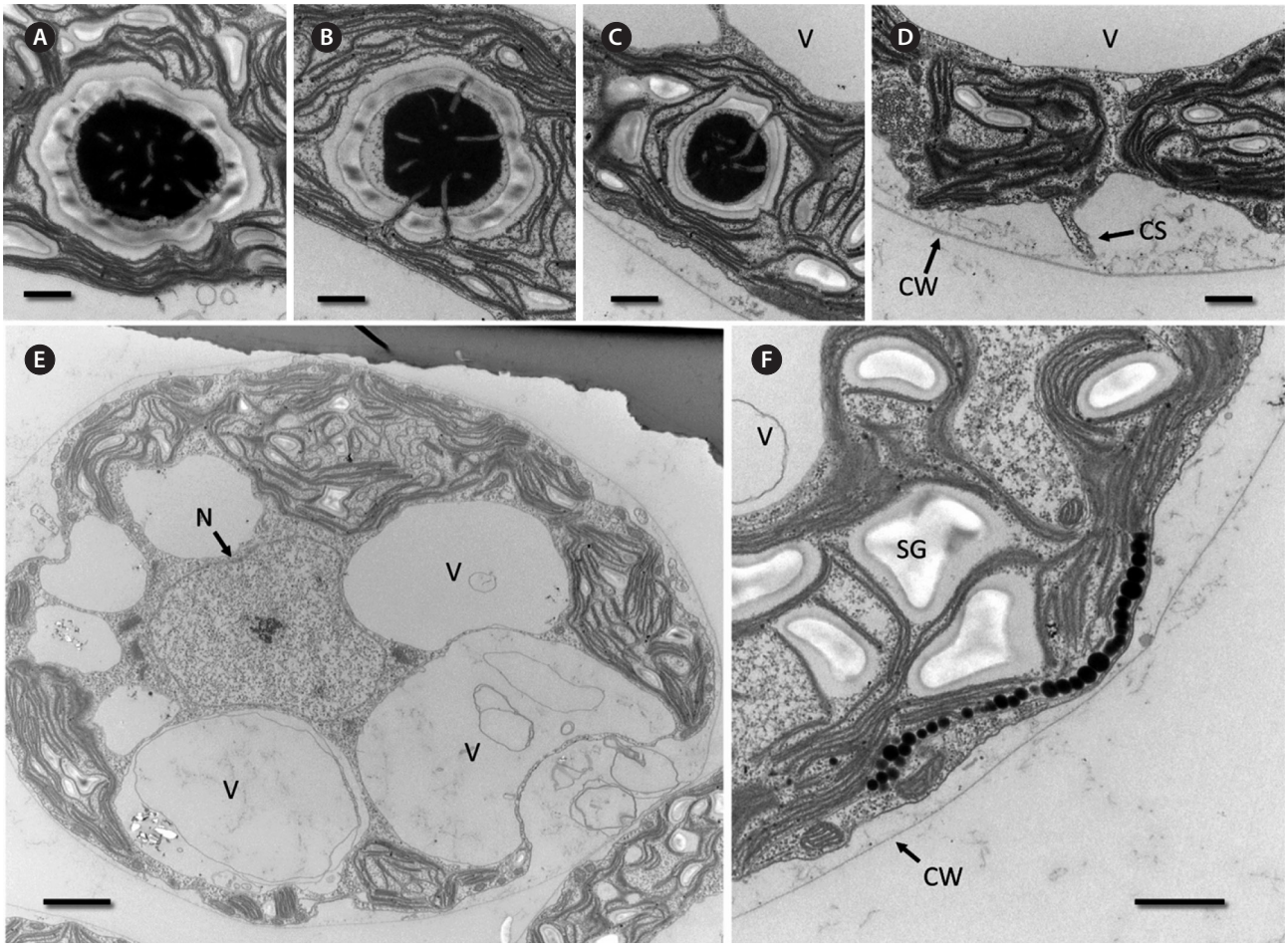

Fig. 2. Transmission electron microscope images for *Haematococcus privus*. (A) Flagellate stage with pyrenoid in chloroplast. (B) Flagellate stage with pyrenoid bearing thylakoids traversing the starch plate through multiple sutures and entering the pyrenoid matrix. (C) Flagellate stage with pyrenoid bearing thylakoids traversing the starch plate through a single suture and entering the pyrenoid matrix. V, vacuole. (D) Flagellate stage illustrating cell boundary with cell wall (CW), cytoplasmic strand (CS), and prominent vacuole (V). (E) Flagellate stage showing entire cell with multiple vacuoles (V) and nucleus (N). (F) Flagellate stage illustrating cell boundary with cell wall (CW), starch grains (SG), and osmiophilic granules of the stigma. Scale bars represent: A–D & F, 800 nm; E, 2 µm.

could not be detected or were few in number (Fig. 1C & E), the corresponding protoplasts were generally larger and manifest a much smaller periplasmic space. The chloroplast is generally cup-shaped, surrounds a central nucleus (Fig. 2E) and bears lobes that appear to be defined, at least in part, by the presence of the large, aqueous vacuoles (Figs 1A, C–E & 2E). Mitochondria are not visible in light micrographs, but numerous small mitochondrial profiles are present on TEM images (Figs 2F, 3A & B). One to six pyrenoids were invariably present (Figs 1A, C [arrows] & 2A–C) and embedded in the chloroplast. Thin sections of pyrenoids revealed multiple starch plates surrounding the pyrenoid matrix (Fig. 2A–C). Tubular invaginations of the pyrenoid matrix (Fig. 2A–C) could be seen to traverse sutures of adjacent starch plates and connect with thylakoids in the chloroplast (Fig. 2B & C). A stigma was not always detected, but when visible, generally appeared as an elongate, acuminate shape (Fig. 1E, arrow). Thin sections revealed a stigma comprised of a single or double layer of osmiophilic globules (Fig. 2F). Motile cells generally contained multiple, large, noncontractile vacuoles (Figs 1A, 1C–E & 2C–F) as well as multiple, small, putative contractile vacuoles (Fig. 1D, arrow). Light microscopy demonstrated that the latter were randomly scattered along the periphery of the protoplast and never observed at the apex of the cell. A flagellar collar was observed at both the light and electron microscope levels (Figs 1B, D & 3A–E). Flagellar collar length is variable with a maximum of ca. 5 µm. Light (Fig. 1B) and electron microscopy (Fig. 3B) suggests that the flagel-

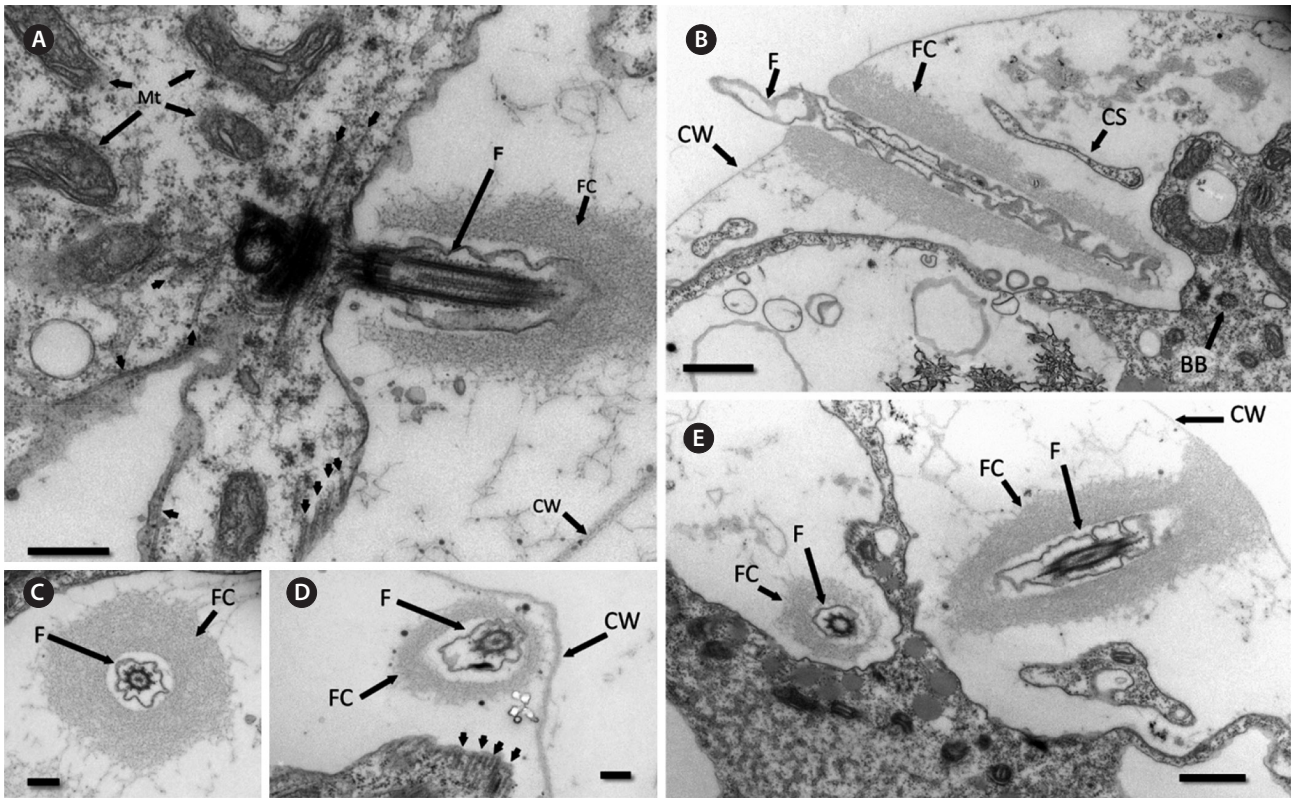

Fig. 3. Transmission electron microscope images for *Haematococcus privus*. (A) Flagellar apparatus with numerous mitochondria (Mt), flagellum (F), basal body, flagellar collar (FC), and cell wall (CW). Flagellar root microtubules are highlighted with arrowheads. (B) Longitudinal section through flagellum (F) projecting through the flagellar collar (FC) and cell wall (CW). Oblique section of a cytoplasmic strand (CS) is visible. BB, basal body. (C) Cross section through flagellum (F) and flagellar collar (FC). (D) Portion of cell wall (CW) is visible. Cytoplasmic microtubules are highlighted with arrows. Cross section through flagellum (F) and flagellar collar (FC). (E) Section showing both flagella, one in cross section and the other in oblique section. Flagella (F) and flagellar collars (FC) are present. Scale bars represent: A, 400 nm; B & E, 800 nm; C & D, 200 nm.

lar collar flares near the cell wall boundary. Thin sections (Fig. 3A–E) indicate a dense, fibrillar nature that is lacking in any regular striations lining the inner wall adjacent to the flagellar axoneme. The flagellar collar is broadly connected with the thin cell wall (Fig. 3B & E) but appears to end before reaching the cell membrane at the base of the flagellum (Fig. 3A & B). Mean flagellar length varied from 17.0 to 20.9 µm (Supplementary Table S2) with a range of 14.9 to 23.5 µm. The ratio of cell length to flagellar length ranged from 1.1 to 2.3. A single section of the flagellar apparatus was observed showing one basal body in transverse section and the second basal body in longitudinal section (Fig. 3A). Putative flagellar root microtubules adjacent to the basal bodies are present (arrows in Fig. 3A & D). Considerable electron dense material is present in the space directly adjacent to the basal bodies (Fig. 3A), but a serious reconstruction of the flagellar apparatus will require evaluation of additional planes of section that is beyond the scope of this investigation.

Mean cell lengths were determined and were always greater than mean cell width for all comparisons (Supplementary Table S2 & Fig. S1A). Mean protoplast length was also always greater than mean protoplast width (Supplementary Table S2 & Fig. S1B). The protoplast length to width ratio varied across all taxa surveyed (Supplementary Table S2) with *H. rubens* (SAG 34-1h) exhibiting a much higher ratio than all other taxa (Supplementary Fig. S2). Results from Wilcoxon Signed-Ranks tests comparing protoplast length and protoplast width confirmed that the difference in protoplast length and width within each taxon or isolate is statistically significant for all taxa or isolates (data not shown). Results from Mann-Whitney U tests indicated that the mean protoplast lengths for each of the three isolates of *Haematococcus* sp. (Pluvialis 5) are not statistically significantly different from one another (Supplementary Fig. S3A). All of the between isolate comparisons of mean protoplast length (Supplementary Fig. S3A) involving *Haematococcus* sp. (Pluvialis 5, the

putative new species, *H. privus*) were statistically significant except for comparisons with *H. rubens* (SAG 34-1h). In addition, comparisons of protoplast length in *H. rubicundus* (SAG 34-1c) with the two *H. lacustris* isolates (SAG 49.94 and NIES-144) failed to detect significant differences. Results from Mann-Whitney U tests indicated that the mean protoplast widths for each of the three isolates of *H. privus* are not statistically significantly different from one another (Supplementary Fig. S3B). None of the between isolate comparisons of mean protoplast width (Supplementary Fig. S3B) involving *H. privus* were statistically significant except for comparisons with *H. rubens* (SAG 34-1h). In fact, only the comparisons of protoplast width involving *H. rubens* (SAG 34-1h) were statistically significantly different (Supplementary Fig. S3B). Results from Mann-Whitney U tests indicated that the ratios of mean protoplast length to mean protoplast width in comparison of the three strains of *H. privus* (HP136, HP137, and HP138) were not statistically significant (Supplementary Fig. S4). The same test demonstrated that all but one of the between isolate comparisons of mean protoplast length to width ratios were statistically significantly different (Supplementary Fig. S4). The one exception was the comparison of ratios for SAG 34-1c (*H. rubicundus*) and NIES-144 (*H. lacustris*) that did not differ significantly (Supplementary Fig. S4).

The green palmella stage is spherical and has acquired a thick cell wall boundary lacking in any appreciable periplasmic space (Fig. 1G & H). Pyrenoids are present at this stage (Fig. 1G), but the cell thickness may obscure them (Fig. 1H). The wall of the motile stage within which palmella cells arise is occasionally present surrounding the palmella cell (Fig. 1H). Bright red pigment accumulation generally proceeds from the center where it presumably surrounds the nucleus which is obscured by the dense cytoplasm (Fig. 1H). Measurements of palmella diameter for HP137 revealed a mean of 19.8 µm with a standard error of the mean of 0.78 µm. No additional comparative data on palmella stage cell diameters and morphometric analyses were prepared for this investigation.

Cells of the akinete stage (often referred to as the aplanospore stage in many recent publications) were generally spherical, varied in diameter (Supplementary Table S2 & Fig. S5), retained the thick cell wall and had accumulated red pigment that fills the entire protoplast (Fig. 1I). Most definitions of the term 'aplanospore' emphasize that the wall of the non-motile stage is not derived from the parent cell. Although this describes the nature of the thick wall that develops in the green, non-motile, palmella stages of *Haematococcus* (see Fig. 1H), it is our opinion that the usage of the term in phycology was intended to describe the production of numerous, non-motile cells in a sporangium. As a consequence, many phycology textbooks refer to the red, thick-walled stage of *Haematococcus* as an 'akinete.' Most phycology texts define the term 'akinete' as a vegetatively-derived, dormant, or resistant stage that bears a wall derived from the parental cell. Thus, the application of the term 'akinete' for the thick-walled red stage of *Haematococcus* is appropriate since one can argue that the thick-walled red stage is the product of development from a thick-walled green (palmella or aplanospore) stage. Pyrenoids are not typically visible with the light microscope in akinetes (Fig. 1I). No akinetes were examined by electron microscopy as part of this investigation.

Results from the Shapiro Wilk test for akinete diameters indicated that most measurement distributions should not be treated as normal. Consequently, all but ANOVA comparisons were completed using non-parametric tests. Mean akinete diameter (Supplementary Table S2 & Fig. S5) varied from 19.55 µm (SAG 49.94) to nearly 32 µm (HP136). Results from Mann-Whitney U tests indicated that the mean akinete diameters for HP136 and HP138 were not statistically significantly different from one another (Supplementary Fig. S6). However, akinete diameters for HP137 vs. HP138 and HP136 vs. HP137 were statistically significantly different (Supplementary Fig. S6). All of the between isolate comparisons of akinete diameter (Supplementary Fig. S6) involving isolates of the putative new species were statistically significant except for one comparison with *H. rubens* (SAG 34-1h vs. HP137). All of the remaining akinete diameter comparisons were statistically significantly different except for the SAG 34-1c vs. SAG 49.94 pairing (Supplementary Fig. S6). Box and whisker plots (Supplementary Fig. S7) are included to illustrate the presence of numerous large outlier akinetes for most strains. If normal distributions are assumed for akinete diameters, single factor ANOVA fails to discriminate three isolates (HP136, HP137, and HP138) of the putative new species (Supplementary Fig. S8A). Single factor ANOVA comparisons of the three isolates with each of the remaining taxa (Supplementary Figs S8B, C & S9) indicate that akinete diameters in *H. privus* are significantly different from akinete diameters for all other isolates / taxa.

18S rRNA phylogeny

Results of phylogenetic analysis of 18S rRNA data (Fig. 4) from a broad sampling of chlamydomonadalean taxa resolved a monophyletic *Haematococcus* plus *E.*

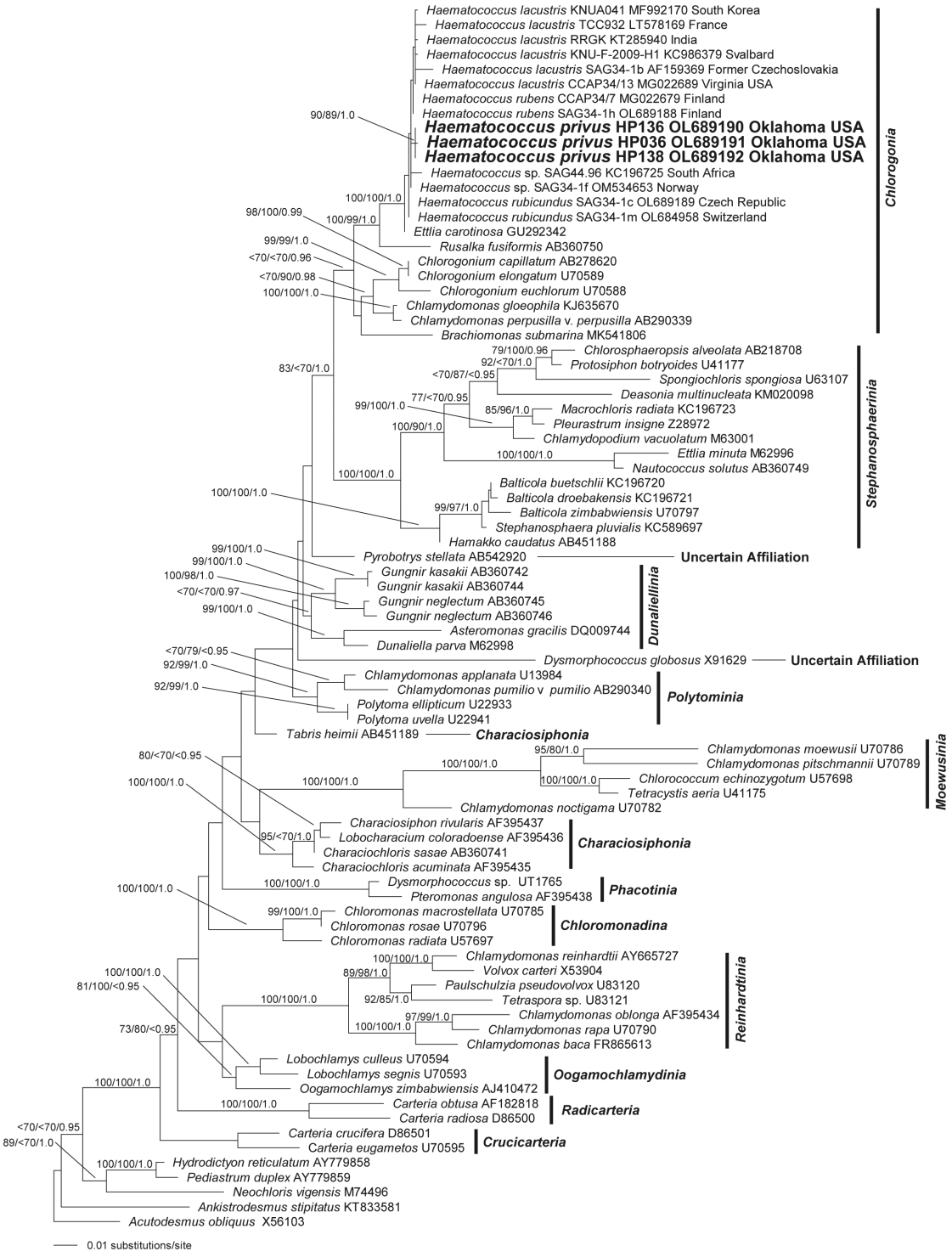

Fig. 4. Phylogeny of *Haematococcus*-based 18S rRNA data from a taxonomically broad sampling of chlamydomonadalean genera. The maximum likelihood (ML) tree was reconstructed using 10 heuristic searches with random taxon addition and the tree bisection-reconnection branch-swapping algorithm as implemented in PAUP*4.0a169 (Swofford 2003) (Model: GTR + I + G; nst = 6; rclass = abcdef; rmatrix = 1.0075713 2.6530925 1.3737438 0.60045607 3.9176836; basefreq = 0.22460816 0.2293864 0.28391317; rates = gamma shape = 0.44499062; pinv = 0.54795489). Data from members of the proposed new species, *H. privus*, are highlighted in boldface. The ML tree is presented with bootstrap proportions (>69) from ML analyses (100 replicates), bootstrap proportions (>69) from neighbor-joining analyses (100 replicates) and posterior probabilities (>0.94) from Bayesian inference are mapped to the corresponding branches. The tree is rooted with data from *Acutodesmus* and *Ankistrodesmus*. Scale bar represents: number of substitutions per site.

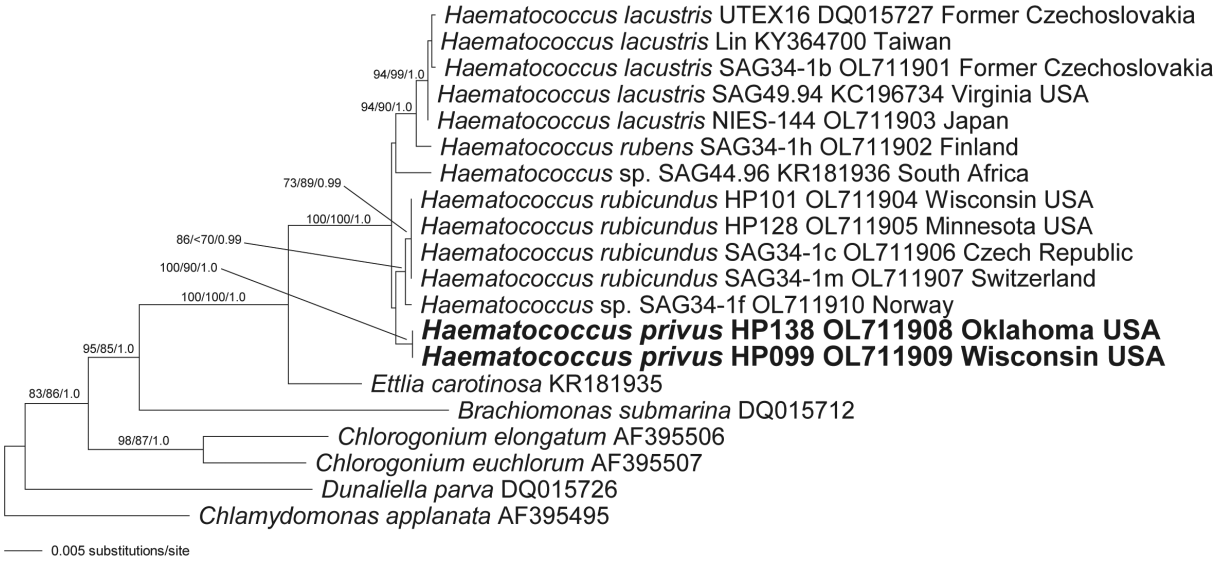

Fig. 5. Phylogeny of *Haematococcus* based on 26S rRNA data from a taxonomically constrained sampling of species and isolates. The maximum likelihood (ML) tree was reconstructed using 10 heuristic searches with random taxon addition and the tree bisection-reconnection branch-swapping algorithm as implemented in PAUP*4.0a169 (Swofford 2003) (Model: TrN + I + G; nst = 6; rclass = abaaca; rmatrix = 1 2.3892541 1 1 7.6413502; basefreq = 0.25978574 0.21583794 0.30357923; rates = gamma shape = 0.64254561 pinv = 0.60988237). Data from members of the proposed new species, *H. privus*, are highlighted in boldface. The ML tree is presented with bootstrap proportions (>69) from ML analyses (100 replicates), bootstrap proportions (>69) from neighbor-joining analyses (100 replicates) and posterior probabilities (>0.94) from Bayesian inference are mapped to the corresponding branches. The tree is rooted with data from *Chlamydomonas applanate*. Scale bar represents: number of substitutions per site.

carotinosa clade with the highest support. *Rusalka* was resolved, with strong support as the sister group to the *Haematococcus* + *Ettlia* alliance (Fig. 4). *Chlorogonium*, *Brachiomonas*, *Chlamydomonas gleophila*, and *Chlamydomonas perpusilla* were allied with *Rusalka*, *Haematococcus*, and *Ettlia* as the Chlorogonia clade (*sensu* Nakada et al. 2008). Only the three *Haematococcus* sp. (*H. privus*) isolates included in the analysis formed a monophyletic group with robust support within the *Haematococcus* and *Ettlia* alliance (Fig. 4).

26S rRNA phylogeny

Results from phylogenetic analysis of 26S rRNA data for a focused set of taxa (principally Chlorogonia taxa) resolved a monophyletic *Haematococcus* with robust support (Fig. 5). *Chlorogonium*, *Brachiomonas*, and *E. carotinosa* form a robust grade with the latter resolved as the sister group to *Haematococcus* (Fig. 5). All *H. lacustris* isolates form a monophyletic group with robust support (Fig. 5). The one strain of *H. rubens* (SAG 34-1h) included in this analysis was resolved with strong support as the sister group to *H. lacustris* (Fig. 5). An unnamed *Haematococcus* isolate from South Africa (SAG 44.96) was resolved as the sister group to the *H. rubens* and *H. lacustris* clade, but without robust support (Fig. 5). All *H. rubicundus* isolates formed a monophyletic group with robust support (Fig. 5). An unnamed *Haematococcus* isolate from Norway (SAG 34-1f) was resolved with robust support as the sister group to *H. rubicundus* (Fig. 5). The two isolates of *H. privus* included in the analysis of 26S rRNA data formed a monophyletic group with robust support. The 26S rRNA data identified the *H. privus* and *H. rubicundus* clades as sister taxa, but the alliance lacks robust support (Fig. 5).

*rbc*L phylogeny

Results from phylogenetic analysis of *rbc*L data for a focused set of taxa (principally Chlorogonia taxa) resolved a monophyletic *Haematococcus* with robust support for ML and BI analyses (Fig. 6). *Brachiomonas*, *Rusalka*, and *E. carotinosa* formed a robust grade with the latter resolved as the sister group to *Haematococcus* (Fig. 6). A monophyletic *Chlorogonium* clade was resolved as sister group to the above alliance, but without robust support (Fig. 6). Data from the sole strain of *H. alpinus* was robustly resolved as the sister group to all remaining isolates of *Haematococcus*. All *H. lacustris* isolates and one *H. rubens* isolate (BE05_11) formed a monophyletic

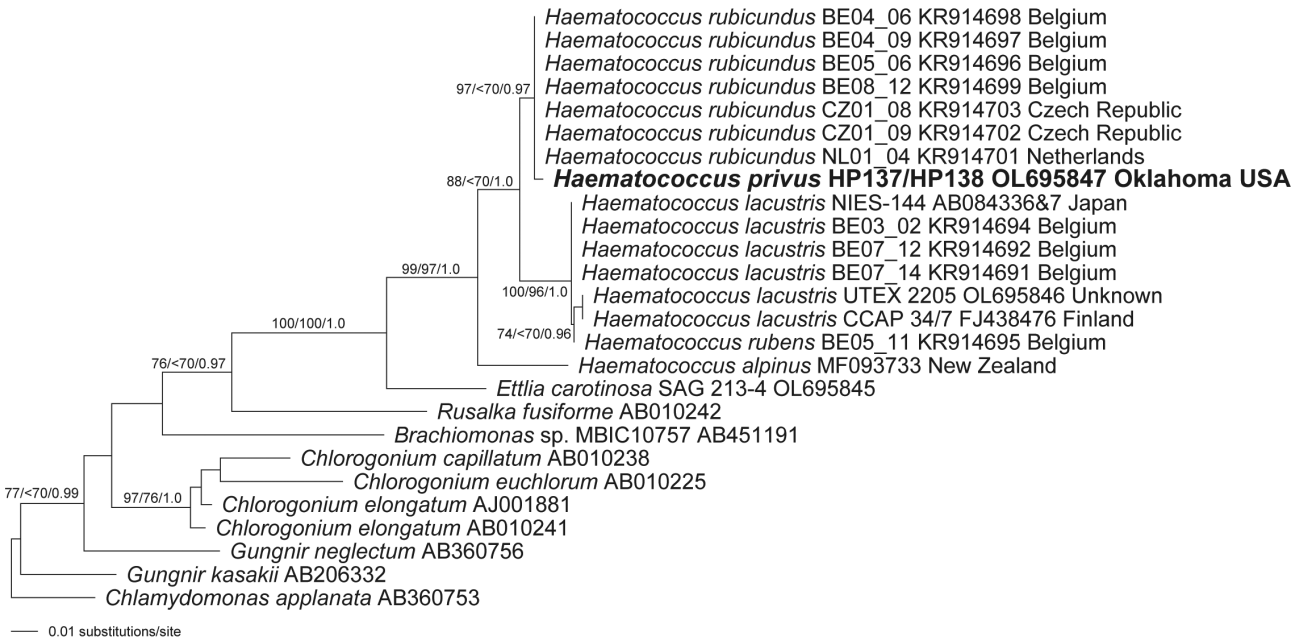

Fig. 6. Phylogeny of *Haematococcus* based on partial *rbc*L data from a taxonomically constrained sampling of species and isolates. The maximum likelihood (ML) tree was reconstructed using 10 heuristic searches with random taxon addition and the tree bisection-reconnection branch-swapping algorithm as implemented in PAUP*4.0a169 (Swofford 2003) (Model: GTR + G; nst = 6; rclass = abcdef; rmatrix = 0.52965762 2.0634922 5.0120517 0.4799857 8.3114761; basefreq = 0.27672136 0.17217936 0.21749192; rates = gamma shape = 0.16518312). Data from a composite taxon derived from partial sequences from two strains representing the proposed new species, *H. privus*, are highlighted in boldface. The ML tree is presented with bootstrap proportions (>69) from ML analyses (100 replicates), bootstrap proportions (>69) from neighbor-joining analyses (100 replicates) and posterior probabilities (>0.94) from Bayesian inference are mapped to the corresponding branches. The tree is rooted with data from *Chlamydomonas applanate*. Scale bar represents: number of substitutions per site.

group with robust support (Fig. 6). The *H. rubens* isolate and two *H. lacustris* isolates (UTEX 2205 and CCAP 34/7) formed a robust sub-clade within the broader *H. lacustris* alliance (Fig. 6). The composite taxon for *H. privus* was robustly resolved as part of a clade that includes all strains of *H. rubicundus* (Fig. 6).

ITS-1 phylogeny

Results from phylogenetic analysis of ITS-1 rRNA data for a focused set of taxa (principally *Haematococcus* taxa) resolved a monophyletic *Haematococcus* with robust support (Fig. 7). *E. carotinosa* was robustly resolved as the sister group to *Haematococcus* (Fig. 7). All isolates of *H. lacustris* were robustly resolved as a monophyletic group (Fig. 7). The data resolve two robust, sub-clades of *H. lacustris* (Fig. 7). One of the *H. lacustris* sub-clades was exclusively comprised of taxa from the White Sea region (Fig. 7). The data resolved the two isolates of *H. rubens* included in the analysis (SAG 34-1h and BE05_11) as the sister group to *H. lacustris* but only the BI analysis exhibited robust statistical support. All isolates of *H. rubicundus* formed a monophyletic group with robust support (Fig. 7). An unnamed isolate from Norway (SAG 34-1f) was resolved, without robust support, as the sister group to the *H. rubicundus* clade. All isolates of the putative new species, *H. privus*, were robustly resolved as a monophyletic group (Fig. 7). The *H. privus* alliance was resolved as sister group to the *H. rubicundus* and *Haematococcus* sp. (SAG 34-1f) alliance but without robust support (Fig. 7). The *H. alpinus* isolate was resolved as the sister taxon to the unnamed *Haematococcus* isolate from South Africa (SAG 44.96) but without robust support. The *H. alpinus* and *Haematococcus* sp. (SAG 44.96) alliance was identified as the sister group to the *H. privus* + *Haematococcus* sp. + *H. rubicundus* alliance but without robust support (Fig. 7).

5.8S rRNA phylogeny

Results from phylogenetic analysis of 5.8S rRNA data for a focused set of taxa (principally *Haematococcus* taxa) resolved a monophyletic *Haematococcus* with robust ($p \geq 0.95$) support from only the BI analysis (Fig. 8). *E. carotinosa* was resolved as the sister group to *Haematococcus*

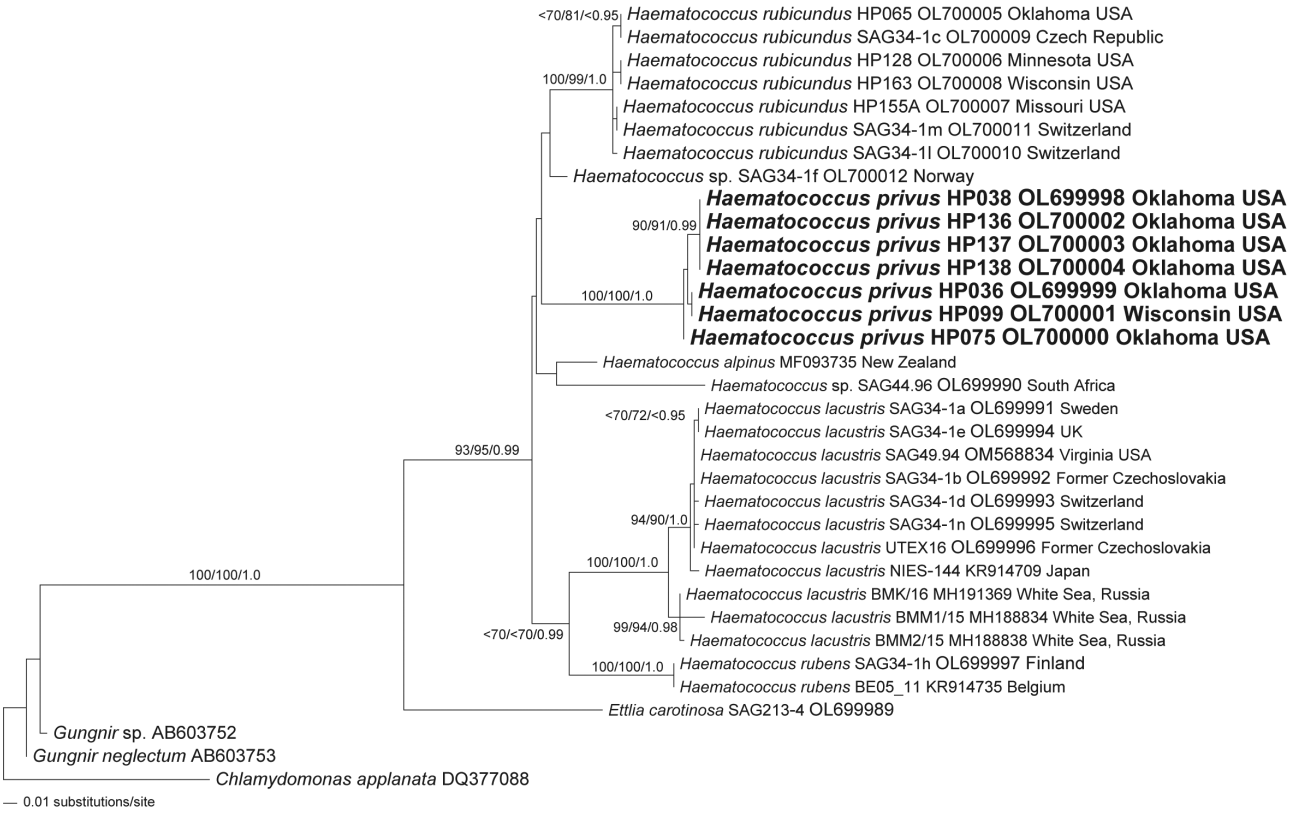

Fig. 7. Phylogeny of *Haematococcus* based internal transcribed spacer-1 data from a taxonomically constrained sampling of species and isolates. The maximum likelihood (ML) tree was reconstructed using 10 heuristic searches with random taxon addition and the tree bisection-reconnection branch-swapping algorithm as implemented in PAUP*4.0a169 (Swofford 2003) (Model: TVM + G; nst = 6 rclass = abcdbe; rmatrix = 1.2383809 4.4338084 2.6430715 0.37224268 4.4338084; basefreq = 0.2040875 0.28227467 0.25382161; rates = gamma shape = 1.0941179). Data from members of the proposed new species, *H. privus*, are highlighted in boldface. The ML tree is presented with bootstrap proportions (>69) from ML analyses (100 replicates), bootstrap proportions (>69) from neighbor-joining analyses (100 replicates) and posterior probabilities (>0.94) from Bayesian inference are mapped to the corresponding branches. Taxa with duplicate sequence data that were excluded from the analysis are listed to the right of the tree and paired, by connecting lines, with the included strain. The tree is rooted with data from *Chlamydomonas applanate*. Scale bar represents: number of substitutions per site.

but only the BI data are robust (Fig. 8). All isolates of *H. lacustris* and *H. rubens* were resolved as a monophyletic group but only the NJ and BI results evidenced strong support (Fig. 8). All isolates of *H. rubicundus*, the two unnamed *Haematococcus* isolates (SAG 44.96 and SAG 34-1f) and the one *H. alpinus* isolate share a node with the *H. lacustris* and *H. rubens* clade but only the BI results were robust (Fig. 8). All isolates of *H. privus* formed a robust, monophyletic group; the *H. privus* clade was the sister group to the remainder of *Haematococcus* species and isolates but only the BI results indicate high statistical probability ($p \geq 0.95$) (Fig. 8).

ITS-2 phylogeny

Results from phylogenetic analysis of ITS-2 rRNA data for a focused set of taxa (principally *Haematococcus* taxa) resolved a monophyletic *Haematococcus* with robust support from only the NJ and BI analyses (Fig. 9). *E. carotinosa* was robustly resolved as the sister group to *Haematococcus* (Fig. 9). All isolates of *H. lacustris* were resolved as a monophyletic group (Fig. 9) but the alliance lacks robust support. The data resolved two sub-clades of *H. lacustris* (Fig. 9). One of the *H. lacustris* sub-clades was exclusively comprised of taxa from the White Sea region (Fig. 9) but support for the sub-clade was robust only for the NJ analysis. All isolates of *H. rubicundus* were allied in a clade with robust support (Fig. 9). The unnamed *Haematococcus* isolate from Norway (SAG 34-1f) was identified as the sister group to *H. rubicundus* but support was not robust (Fig. 9). The *H. alpinus* isolate and the unnamed *Haematococcus* isolate from South Africa (SAG

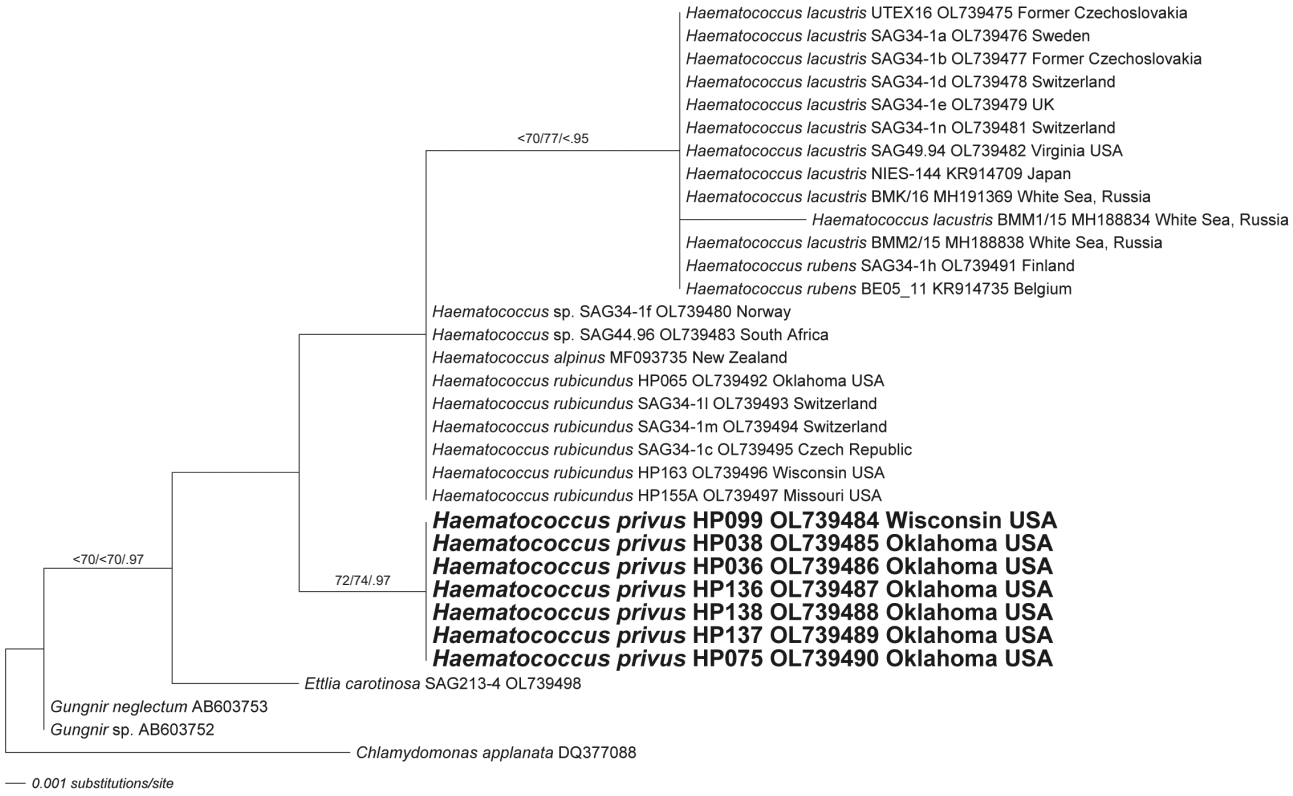

Fig. 8. Phylogeny of *Haematococcus* based 5.8S rRNA data from a taxonomically constrained sampling of species and isolates. The maximum likelihood (ML) tree was reconstructed using 10 heuristic searches with random taxon addition and the tree bisection-reconnection branch-swapping algorithm as implemented in PAUP*4.0a169 (Swofford 2003) (Model: K80; tratio = 10.119339; basefreq = equal). Data from members of the proposed new species, *H. privus*, are highlighted in boldface. The ML tree is presented with bootstrap proportions (>69) from ML analyses (100 replicates), bootstrap proportions (>69) from neighbor-joining analyses (100 replicates) and posterior probabilities (>0.94) from Bayesian inference are mapped to the corresponding branches. The tree is rooted with data from *Chlamydomonas applanate*. Scale bar represents: number of substitutions per site.

44.96) were resolved as sister taxa but the alliance was not robust (Fig. 9); this clade was identified as the sister group to the *H. rubicundus* + *Haematococcus* sp. (SAG 34-1f) alliance but the support was not robust (Fig. 9). All isolates of the putative new species, *H. privus,* were robustly resolved as a monophyletic group (Fig. 9). The *H. privus* alliance was resolved, without robust support, as the sister group to the *H. alpinus* + *Haematococcus* sp. (SAG 44.96) + *Haematococcus* sp. (SAG 34-1f) + *H. rubicundus* clade (Fig. 9). The two isolates of *H. rubens* (SAG 34-1h and BE05_11) were robustly resolved as a monophyletic group (Fig. 9) which were, in turn, resolved as the sister to the *H. privus* + *H. alpinus* + *Haematococcus* sp. (SAG 44.96) + *Haematococcus* sp. (SAG 34-1f) + *H. rubicundus* clade, but without robust support (Fig. 9).

Carotenoid content

Results of the pigment induction experiments failed to reveal any obvious differences in the amounts and types of carotenoids for the four strains examined (Supplementary Fig. S10). Results from cell counts (Fig. 10A) indicated that the experimental conditions produced the highest, mean cell density in *H. rubicundus* (SAG 34-1c; ca 5.5 × 10^5 cells mL^{-1}) and the lowest in *H. privus* (HP136; ca 1.7 × 10^5 cells mL^{-1}). The values for cell density were statistically significantly different (ANOVA cell count ~ Isolate; $F_{4,10}$ = 4.308, p = 0.0278; Tukey honestly significant difference SAG 34-1c vs. HP136; p = 0.0181).

Although the mean for total carotenoid yield was highest in *H. rubicundus* (SAG 34-1c) at 14.32 µg per 10^5 cells, this difference was not statistically significant from the other strains ($F_{4,10}$ = 0.371, p = 0.824) (Fig. 10B). The total carotenoid yield did not vary greatly between the remaining strains with a mean of ca. 8 µg per 10^5 cells (Fig. 10B). Astaxanthin was the most abundant carotenoid type in all strains ranging from 62.7 to 67.9% of total carotenoid content. The mean for total astaxanthin yield was high-

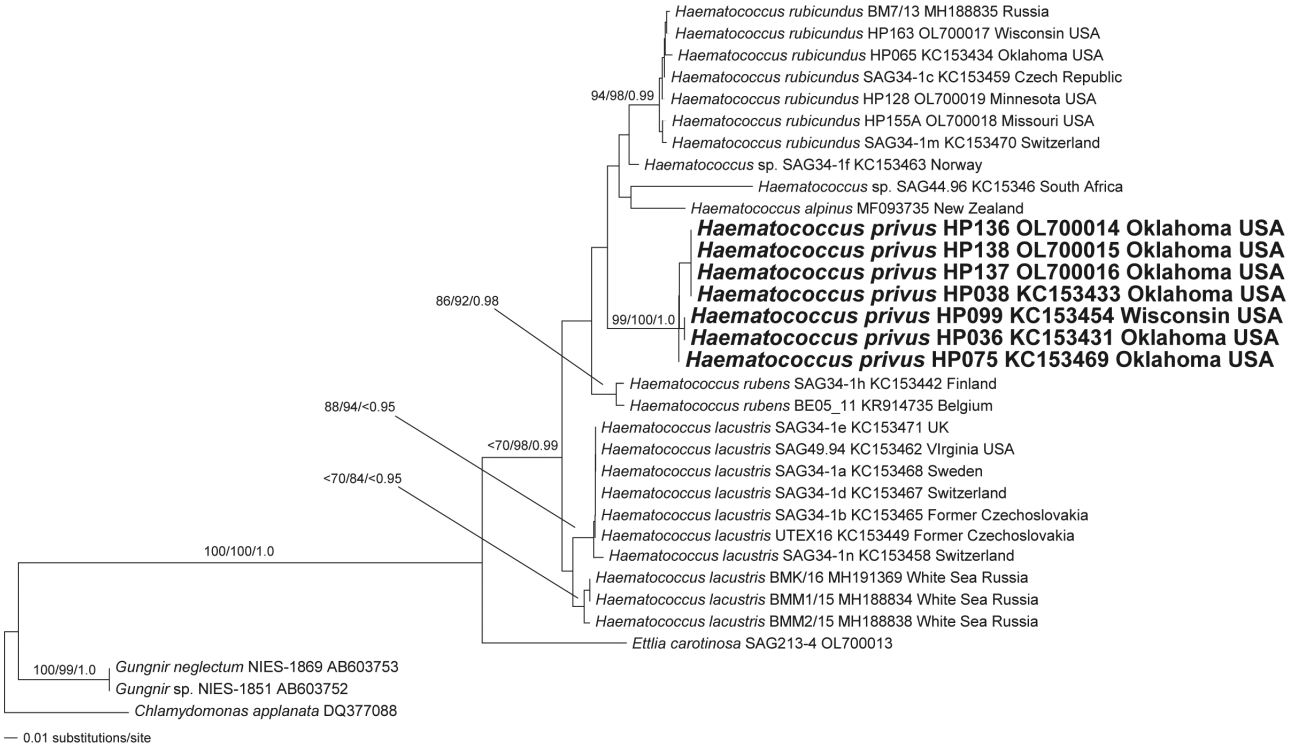

Fig. 9. Phylogeny of *Haematococcus* based on a manually-adjusted, secondary structure-guided alignment of internal transcribed spacer-2 data from a taxonomically constrained sampling of species and isolates. The maximum likelihood (ML) tree was reconstructed using 10 heuristic searches with random taxon addition and the tree bisection-reconnection branch-swapping algorithm as implemented in PAUP*4.0a169 (Swofford 2003) (Model: SYM + G; nst = 6; rclass = abcdef; rmatrix = 3.1124081 5.8032147 3.5500665 0.68624069 10.534802; gamma shape = 1.0425506). Data from members of the proposed new species, *H. privus*, are highlighted in boldface. The ML tree is presented with bootstrap proportions (>69) from neighbor-joining (NJ) analyses (100 replicates), bootstrap proportions (>69) from NJ analyses (100 replicates) and posterior probabilities (>0.94) from Bayesian inference are mapped to the corresponding branches. The tree is rooted with data from *Chlamydomonas applanate*. Scale bar represents: number of substitutions per site.

est in *H. rubicundus* (SAG 34-1c) at 9.58 µg per 10^5 cells, but was not statistically significantly greater than other strains ($F_{4,10}$ = 0.393, p = 0.809) (Fig. 10C). The mean total for astaxanthin yield did not vary greatly between the remaining strains with a mean of ca. 6 µg per 10^5 cells (Fig. 10C).

DISCUSSION

Light microscopy

The basic features of the motile stage (Fig. 1A–E) and akinete stage (Fig. 1H & I) of *H. privus* (sp. nov.) vary little from the other recognized species of *Haematococcus*. Similarly, the palmella stage (Fig. 1G) does not appear to be distinct, but no comparative measurement data were recorded for this stage. However, simple morphometric analyses of the motile stage indicate that the ratio of protoplast length to width distinguishes *H. privus* from all isolates in the comparison (Supplementary Figs S2 & S4). In addition, akinete diameters in *H. privus* are generally larger than the comparison group save for *H. rubens* (Supplementary Figs S5–S7) under the indicated culturing conditions. These measurement data, for the motile cells in particular, will require further testing that takes into account possible influence of development or time of day.

Transmission electron microscopy

Ultrastructural features of the *H. privus* motile cell are generally similar to observations recorded in previous investigations of *Haematococcus*. Specifically, pyrenoid ultrastructure in *H. privus* appears to be similar to that in *H. alpinus* (Mazumdar et al. 2018), *H. lacustris* (Santos and Mesquita 1984, Damiani et al. 2006, Pegg et al. 2015, unpublished observations) and *E. carotinosa* (Pegg et al.

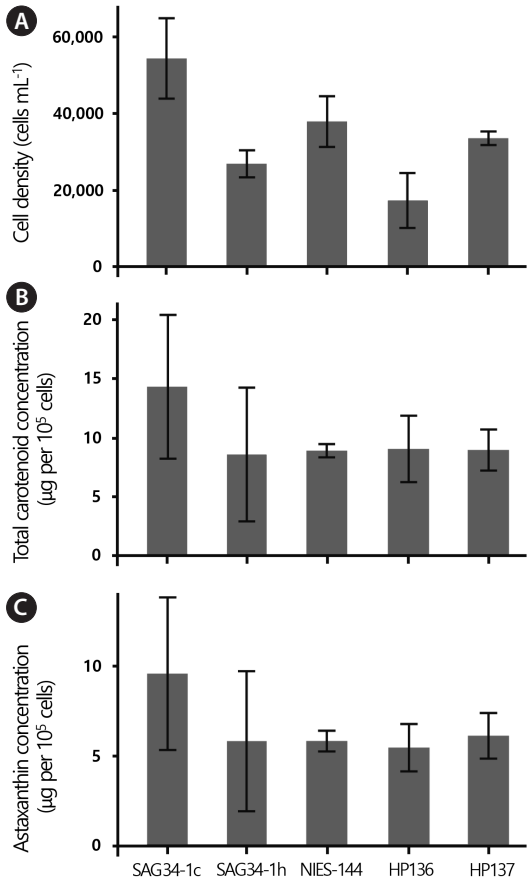

Fig. 10. Cell counts, total carotenoid yield and total astaxanthin yield following 14-day period of carotenoid induction for five strains of *Haematococcus* (SAG 34-1c = *H. rubicundus*, SAG 34-1h = *H. rubens*, NIES-144 = *H. lacustris*, HP136 and HP137 = *H. privus*) . Error bars represent ± standard deviation values. (A) Cell count data (cells mL^{-1}). (B) Total carotenoid yield (µg per 10^5 cells). (C) Total astaxanthin yield (µg per 10^5 cells).

2015). However, our TEM data provide new insights into the unusual flagellar collar in *Haematococcus*, a structure that was first noted by Hazen (1899) and Herrick (1899). Although similar structures have been detailed in *Chlamydomonas* (Ringo 1967, Harris 2009), the flagellar collar in *Haematococcus* is much longer than that in *Chlamydomonas* simply because the distance between protoplast and cell wall differs greatly between the two species. The first ultrastructural investigation of the flagellar collar (or flagellar tube) was reported by Bowen (1964) who noted that these structures were observed in *Haematococcus* and *Balticola* Droop, both of which have substantive periplasmic spaces between the cell wall and protoplast. However, the flagellar collars of *Haematococccus* were much longer even than those observed in *Balticola* (Bowen 1964). A comparison of light microscopic data (unpublished observations) indicates that the flagellar collar of *H. privus* appears to be similar to that in other species or lineages of *Haematococcus*. However, the length of these unusual features seems likely to vary as motile cells enlarge during maturation towards non-motile phases. At least some sporangia of *H. privus* (like other species of *Haematococcus*) remain motile during zoosporogenesis where one of the daughter cells may retain the parental flagella (Pocock 1960). The development and fate of the flagellar collar during motile cell maturation and sporogenesis requires further investigation.

Molecular phylogeny

Results from the phylogenetic analyses presented here support the view that *Haematococcus* is comprised of at least five distinct, species-level lineages (Allewaert et al. 2015, Mazumdar et al. 2018). All of the ribosomal markers (Figs 4, 5 & 7–9) robustly identify the *H. privus* isolates as comprising a lineage that is distinct among all other *Haematococcus* isolates including representatives of the four, currently-recognized species, *H. alpinus*, *H. lacustris*, *H. rubens*, and *H. rubicundus*. Of particular note are the results from 18S rRNA data analysis. As noted in the Introduction, the 18S rRNA data have shown little variation among isolates of *Haematococcus* (Buchheim et al. 2013, Klochkova et al. 2013, Pegg et al. 2015, Kim et al. 2021) and was largely abandoned by us in favor of collecting data from the ribosomal spacers. The results presented here still indicate that the 18S rRNA gene exhibits little variation among all *Haematococcus* isolates plus *E. carotinosa* (overall mean p-distance = 0.002). Thus, it is noteworthy that phylogenetic analysis of 18S rRNA provides robust support (albeit from just two informative sites) only for the *H. privus* alliance (Fig. 4).

Our results also confirm that *E. carotinosa* is the closest ally of *Haematococcus,* but deserves to retain its taxonomic status as part of a distinct genus. In addition to the five lineages currently comprised of named *Haematococcus* species (*H. alpinus*, *H. lacustris*, *H. privus* [sp. nov.], *H. rubens*, and *H. rubicundus*), our data also affirm that *Haematococcus* sp. (SAG 34-1f) is distinct from the named lineages and is likely destined to be described as new species. Another unnamed strain (SAG 44.96) is phenetically distinct from other lineages, but ITS-1 (Fig. 7) and ITS-2 (Fig. 9) data indicate a possible sister status with *H. alpinus*.

While the ribosomal data identified *H. privus* as distinct, the *rbc*L data placed the composite taxon representing *H. privus* as an ally in the *H. rubicundus* clade (Fig.

6). Unfortunately, this result must be regarded with some caution since it is based on a composite sequence that is also relatively short (see below). On the other hand, the 26S rRNA data (Fig. 5), the ITS-1 data (Fig. 7), and the ITS-2 data (Fig. 9) identify *H. privus* and *H. rubicundus* as sister taxa. While support for this alliance of *H. privus* and *H. rubicundus* is weak, none of the ribosomal analyses offers a robust assessment identifying any other lineage as the sister group to *H. privus*. Thus, the *rbc*L tree may not be in conflict with the ribosomal data.

*rbc*L anomalies

Our results with *rbc*L require special mention in that our amplification efforts frequently failed to produce a workable product despite using a variety of primers designed for chlorophycean flagellates in general (Nozaki et al. 1995) or specifically for *Haematococcus* (Kim et al. 2015). For example, to date, we have been unable to produce an *rbc*L amplification product for SAG 34-1f (*Haematococcus* sp.) or SAG 44.96 (*Haematococcus* sp.). Although these failures may be a consequence of our somewhat limited experience with *rbc*L, two lines of evidence indicate that the chloroplast genome of *Haematococcus* is unusual. Genomic studies recently identified *Haematococcus* as possessing what may be the largest chloroplast genome on record at more than a megabase (Bauman et al. 2018, Smith 2018). In addition, our experience with *rbc*L amplification suggests that the chloroplast genomes of *E. carotinosa* and *H. privus* likely bear some interesting features given that the PCR product size was anomalous (see Materials and Methods). Furthermore, the nuclear ribosomal data identify SAG 34-1f and SAG 44.96 as comprising distinct branches (Allewaert et al. 2015, present investigation). Resolving the problems associated with obtaining homologous *rbc*L reads is certainly needed to help with the possible phylogenetic conflict between plastid and nuclear ribosomal data. Moreover, it will likely be necessary to sample many more markers (nuclear, plastid, and mitochondrial) to address the potential conflict between datasets. Obtaining chloroplast genome data from other lineages has huge potential to aid in understanding the origins of the large genome in *H. lacustris* (and perhaps other lineages) and likely will provide additional clarity on phylogeny of the genus.

Carotenoid analyses

Allewaert et al. (2017) found considerable variability in carotenogenesis among numerous strains of *H. lacustris* and *H. rubicundus*. The data we presented here is based on a much smaller set of strains and our induction protocol (starting with exponential stage motile cells rather than stationary stage palmella; high light and reduced phosphate rather than just reduced phosphate) and analysis protocol (HPLC rather than spectrophotometry) differed from that of Allewaert et al. (2017). Allewaert et al. (2017) noted that astaxanthin production could be relatively high in *H. rubicundus* (e.g., CZD1_08), but higher rates for astaxanthin productivity were reported in strains of *H. lacustris* (e.g., BE02_09). The remaining strains in our analysis did not show unambiguous differences in total carotenoid and astaxanthin yields (Fig. 10B & C). On the other hand, cell counts indicate that the strains we studied exhibited different rates of cell division under our induction conditions (Fig. 10A). Again, *H. rubicundus* (SAG 34-1c) showed the highest average growth rate of all strains in our analysis. This result appears to be consistent with observations by Allewaert et al. (2017) where more strains of *H. rubicundus* than *H. lacustris* showed relatively high growth rates. Researchers focused on optimizing astaxanthin production for commercialization generally must first enhance growth of *Haematococcus* and then, alter conditions that favor carotenogenesis (e.g., Rizzo et al. 2022). Thus, a strain that has both high growth rates and high astaxanthin productivity is desirable. Despite high values for variance, our carotenoid yields suggest that *H. rubicundus* (SAG 34-1c) is worthy of additional study as a possible source for astaxanthin and other valuable pigments (Fig. 10B & C).

Development

Reproduction in all strains of *H. privus* was characterized by asexual means only. When routinely (every 3 weeks) sub-cultured into fresh medium, the motile stage remains the dominant form. As the culture ages, motility is lost and cells transition to green palmella and eventually red akinetes. No sexual reproductive stages (i.e., microzooids *sensu* Hazen 1899) were ever detected. A number of early researchers reported gametogenesis, syngamy, zygote formation, and zygote germination in *Haematococcus* (Peebles 1909, Schulze 1927). Droop (1956) concluded that sexual reproduction in *Haematococcus lacustris* is heterothallic which may account for the rarity of sexuality in the laboratory. Nonetheless, Droop (1956) and other researchers concluded that *Haematococcus* is rarely if ever sexual (Hazen 1899, Herrick 1899, Elliott 1934, Pocock 1960). Most recently, Triki et al. (1997) and Bai et al. (2016) reported gametogenesis in *Haemato-*

coccus but neither found evidence of syngamy. It seems likely that *Haematococcus* has retained at least some of the genetic machinery for gametogenesis, but the resistant, akinete stage removes or reduces the need to produce zygotes as a means to survive extreme conditions. If, as the evidence suggests, *Haematococcus* reproduction is largely or exclusively asexual, then one may ask whether the *Haematococcus* lineage is affected by Muller's ratchet (Muller 1932). A time-calibrated phylogeny indicated that the lineage that includes *Haematococcus* and the lineage that contains the sister genus, *Rusalka* (see Fig. 4), diverged no more recently than 45 million years ago (Munakata et al. 2016). Thus, it seems perfectly legitimate to question why this relatively ancient lineage is resistant to Muller's ratchet.

The issue of sexuality in *Haematococcus* is obscured, though, as a consequence of several studies that reported doubling (or more) of DNA content during what is ostensibly vegetative development. Lee and Ding (1994) reported that cells of *H. lacustris* UTEX 16 underwent fusion at a point in the cell cycle where the zoospores ceased dividing and that this corresponded to a doubling of DNA content in most cells. Since no micrographs illustrating cell fusion were presented it appears that cell fusion was inferred from the increase in DNA content. This conclusion is further supported by a passage in the Results section "…Fusion of cells (i.e., doubling in DNA content) was observed between 65 and 113 h of incubation…" (Lee and Ding 1994). The only detailed report of motile cell (macrozoid) fusion or syngamy (Peebles 1909) was rejected by most other investigators who noted that *Haematococcus* is prone to produce motile cells that are the product of incomplete cytokinesis and that fusion was only associated with gametes or microzooids (Pocock 1960). Even if this phenomenon is unlikely to be the product of fusion or syngamy, the DNA doubling requires explanation. Reinicke et al. (2018) studied development in *H. lacustris* and concluded that this alga exhibits a hybrid form of cell cycle that is intermediate between the *Chlamydomonas* type and the *Scenedesmus* type. Of particular note is the observation that the *H. lacustris* cell cycle is characterized by a transient polyploid phase where genome duplication may be as much as or even more than 16C (Reinicke et al. 2018). Following the polyploid phase, the cells of *H. lacustris* proceeded to mitosis and a transient polynuclear phase in the palmella or aplanospore stage and finally cytokinetic production of individual motile cells (Reinicke et al. 2018). Reinicke et al. (2018) suggested that the polyploid phase may be a large factor in genome expansion in *Haematococcus*. Polyploidy has also been proposed as a mechanism that organisms might exploit to escape Muller's ratchet through gene conversion (Maciver 2016). The most famous case of organisms escaping Muller's ratchet, the Bdelloid rotifers, may also be using gene conversion due to polyploidy to eliminate deleterious mutations (Flot et al. 2013). Thus, polyploidy in *Haematococcus* may explain how it escapes Muller's ratchet while simultaneously offering an explanation for the relatively high level of intragenomic variation in the ITS-2 ribosomal spacer in numerous lineages of *Haematococcus* (Alanagreh et al. 2017).

Biogeography

The scope of sampling for *Haematococcus* diversity remains rather narrow. For example, Africa and Asia remain largely unsampled with respect to available cultures. We know from the work of Pocock (1960) that southern Africa had a myriad of collecting sites for *H. lacustris*. Unfortunately, we are not aware of any extant material from the Pocock surveys. Europe, North America, and South America have the most sampling records at the moment. The limited sampling that has been done indicates that *H. lacustris* and *H. rubicundus* are distributed on a global scale. Of those two, *H. lacustris* is the most frequently sampled lineage and our data indicate that it also exhibits the greatest amount of molecular diversity among the recognized species where taxon sampling includes at least six lineages. Maximum within group p-distance for ITS-1 data was 0.043, 0.000, and 0.011 for *H. lacustris*, *H. rubicundus*, and *H. privus*, respectively. Maximum within group p-distance for ITS-2 data was 0.026, 0.005, and 0.010 for *H. lacustris*, *H. rubicundus*, and *H. privus*, respectively. In addition, the data from both internal transcribed spacers (Figs 7 & 9) indicate that a number of White Sea polar isolates (Chekanov et al. 2020) form a sub-clade within *H. lacustris*. Although the support for the White Sea clade is weakest with the ITS-2 data (Fig. 9), the ITS-1 data resolve this alliance with robust support (Fig. 7). This lineage may be worthy of elevation to formal status as a variety of *H. lacustris*.

The principal finding from this investigation is that a new species of *Haematococcus* has been discovered and described. The new species, *H. privus*, is currently known only from Oklahoma and Wisconsin (USA). This brings to five, the number of recognized species of *Haematococcus* that have been characterized at the molecular level. These new observations regarding *Haematococcus* diversity will aid in the interpretation of any differences in carotenoid production and yield that may have a phylogenetic

component. In light of the expanding range of diversity in the genus *Haematococcus* coupled with morphological overlap, we recommend that researchers focused on carotenogenesis confirm the phylogenetic status of any new strain by sequencing the ITS array. Lastly, we point out that there are a number of interesting features of *Haematococcus* (chloroplast genome expansion, nuclear polyploidy, presence or absence of sexuality) that should further stimulate interest in a basic science investigation of this alga. Addressing questions regarding these developmental phenomena is also likely to have relevance for applied studies of *Haematococcus*.

Species description

Haematococcus privus **Buchheim sp. nov. (Figs 1–10, Supplementary Figs S1–S7).**

Description. Motile vegetative cells generally ovoid to subspherical (as cells mature), average 29.0 µm long (range 19.2–42.5 µm), 24.9 µm wide (range 14.5–36.9 µm). A single wall papillum may be present. Average protoplast length 22.9 µm (range 15.4–33.0 µm) and average width 18.4 µm (range 11.4–28.3 µm) that generally bore a plasma papillum where the two flagella are inserted at angles normally less than 90°. Cytoplasmic strands generally present, mostly branched near the wall and distributed over the entire protoplast. Two isokont anterior flagella present, these generally shorter than the cell length (ratio of cell length to flagellar length = 1.3) when measured from wall insertion to tip. Flagella in the periplasmic space are surrounded by short divergent collars comprised of fibrillar material, up to 5 µm in length, that originate from the inner wall and terminate near the protoplast but are not connected directly to the protoplast. Chloroplast cup-shaped, occupying the bulk of the periphery of the protoplast and containing 1–6 scattered spherical pyrenoids. Contractile vacuoles numerous, scattered along the periphery of the protoplast. Nucleus centrally located and often surrounded by numerous vacuoles of varied size and may be surrounded partially or completely by red pigment. Cells lose their flagella, acquire a thick cell wall, gradually increase in size, eventually turning red / orange and forming a resistant, round akinete enclosed by a thick cell wall. Average diameter of mature akinetes (red) 30.2 µm (range 16.7–65 µm). Found in small, temporary water pools or puddles. Differs in *rbc*L, 18S rRNA, ITS-1, 5.8S rRNA, and ITS-2 sequence from *H. alpinus*, *H. lacustris*, *H. rubens*, and *H. rubicundus*. Differs in 26S rRNA sequence from *H. lacustris*, *H. rubens*, and *H. rubicundus*. Motile and non-motile stages are morphologically similar to and overlapping with *H. lacustris*, *H. rubens*, and *H. rubicundus*. On average, protoplasts of motile cells had a greater length : width ratio and greater akinete diameter than *H. lacustris*, *H. rubens*, and *H. rubicundus*. The protoplast apex was more often acuminate forming a plasma papillum. No sexual stages were observed.

Holotype. Strain HP136 collected by Buchheim M.

Type locality. From a water puddle on a karst, limestone outcrop beneath a canopy of deciduous trees; Tulsa, OK, USA (36°13.217′ N, 95°47.914′ W).

Etymology. *privus* (Latin for rare, uncommon, and distinctive) for its limited distribution.

GenBank accession number. 18S rRNA (OL689190), 26S rRNA (OL711908); ITS1 (OL700002), 5.8S rRNA (OL739487), ITS2 (OL700014).

Additional material. Strains HP137 and HP138.

Distribution. Specimens were found in the United States.

ACKNOWLEDGEMENTS

The authors wish to thank Ian Bellovich, Claire Chapman, Karina Cunningham, Marwa Elsayed, Michaelyn Everitt, Anna-Maria Malati, Ashley Lam, Chukwunonso Nwakoby, Kelsey Parks, Caitlin Pegg and Sydney Sullivan who assisted with DNA extraction, PCR and microscopy. The authors acknowledge support from the Oklahoma Center for the Advancement of Science and Technology (PS20-021: Bioprospecting Oklahoma's Algal Diversity For High Value Products).

CONFLICTS OF INTEREST

The authors declare that they have no potential conflicts of interest.

SUPPLEMENTARY MATERIALS

Supplementary Table S1. *Haematococcus* and *Ettlia* taxa included in the various analyses conducted for this investigation (https://www.e-algae.org).

Supplementary Table S2. Morphometric data recorded by light microscopy for three isolates of *Haematococcus privus*, two isolates of *H. lacustris*, one isolate of *H. rubens* and one isolate of *H. rubicundus* (https://www.e-algae.org).

Supplementary Fig. S1. Mean width and length of mo-

tile cell (A) and protoplast (B) (https://www.e-algae.org).

Supplementary Fig. S2. Ratios of mean protoplast length (motile cell) to protoplast width (motile cell) (https://www.e-algae.org).

Supplementary Fig. S3. Mann-Whitney U test: comparison of mean protoplast length (A) and width (B) (motile cells) (https://www.e-algae.org).

Supplementary Fig. S4. Mann-Whitney U test: comparison of protoplast length to width ratios (motile cells) (https://www.e-algae.org).

Supplementary Fig. S5. Mean akinete diameter (https://www.e-algae.org).

Supplementary Fig. S6. Mann-Whitney U test: comparison of akinete diameters (https://www.e-algae.org).

Supplementary Fig. S7. Box and whisker plots for akinete diameter (https://www.e-algae.org).

Supplementary Fig. S8. ANOVA single factor analysis of akinete diameter variance for the three isolates of *Haematococcus privus* (A), *H. rubens* (B), and *H. rubicundus* (C) (https://www.e-algae.org).

Supplementary Fig. S9. ANOVA single factor analysis of akinete diameter variance for the three isolates of *Haematococcus privus* and *H. lacustris* (A, NIES-144; B, SAG 49.94) (https://www.e-algae.org).

Supplementary Fig. S10. Representative chromatograms from high-performance liquid chromatography analysis of six *Haematococcus* strains at 480 nm normalized to the astaxanthin peak (https://www.e-algae.org).

REFERENCES

Ahirwar, A., Meignen, G., Khan, M. J., Sirotiya, V., Harish, Scarsini, M., Roux, S., Marchand, J., Schoefs, B. & Vinayak, V. 2021. Light modulates transcriptomic dynamics upregulating astaxanthin accumulation in *Haematococcus*: a review. Bioresour. Technol. 340:125707.

Alanagreh, L., Pegg, C., Harikumar, A. & Buchheim, M. 2017. Assessing intragenomic variation of the internal transcribed spacer two: adapting the Illumina megagenomics protocol. PLoS ONE 12:e0181491.

Allewaert, C. C., Vanormelingen, P., Daveloose, I., Verstraete, T. & Vyverman, W. 2017. Intraspecific trait variation affecting astaxanthin productivity in two *Haematococcus* (Chlorophyceae) species. Algal Res. 21:191–202.

Allewaert, C. C., Vanormelingen, P., Pröschold, T., Gómez, P. I., González, M. A., Bilcke, G., D'Hondt, S. & Vyverman, W. 2015. Species diversity in European *Haematococcus pluvialis* (Chloophyceae, Volvocales). Phycologia 54:583–598.

Ankenbrand, M. J., Keller, A., Wolf, M., Schultz, J. & Förster, F. 2015. ITS2 database V: twice as much. Mol. Biol. Evol. 32:3030–3032.

Ashokkumar, V., Chen, W. -H., Kumar, G., Satjarak, A., Chanthapatchot, W. & Ngamcharussrivichai, C. 2021. A biorefinery approach for high value-added bioproduct (astaxanthin) from alga *Haematococcus* sp. and residue pyrolysis for biochar synthesis and metallic iron production from hematite (Fe_2O_3). Fuel 304:121150.

Bai, N. J., Nair, B. B. & Shashirekha, V. 2016. Biology of growth conditions, nutrition and biomass development in *Haematococcus pluvialis*, Haematococcaceae, Chlorophyceae. Phykos 46:64–70.

Bauman, N., Akella, S., Hann, E., Morey, R., Schwartz, A. S., Brown, R. & Richardson, T. H. 2018. Next-generation sequencing of *Haematococcus lacustris* reveals an extremely large 1.35-megabse chloroplast genome. Genome Announc. 6:e00181–18.

Bowen, W. R. 1964. Ultrastructural aspects of the cell boundary of *Haematococcus pluvialis*. Trans. Am. Microsc. Soc. 86:36–43.

Buchheim, M. A., Kirkwood, A. E., Buchheim, J. A., Verghese, B. & Henley, W. J. 2010. Hypersaline soil supports a diverse community of *Dunaliella* (Chlorophyceae). J. Phycol. 46:1038–1047.

Buchheim, M. A., Michalopulos, E. A. & Buchheim, J. A. 2001. Phylogeny of the Chlorophyceae with special reference to the Sphaeropleales: a study of 18S and 26S rDNA data. J. Phycol. 37:819–835.

Buchheim, M. A., Sutherland, D. M., Buchheim, J. A. & Wolf, M. 2013. The blood alga: phylogeny of *Haematococcus* (Chlorophyceae) inferred from ribosomal RNA gene sequence data. Eur. J. Phycol. 48:318–329.

Buchheim, M., Buchheim, J., Carlson, T., Braband, A., Hepperle, D., Krienitz, L., Wolf, M. & Hegewald, E. 2005. Phylogeny of the Hydrodictyaceae (Chlorophyceae): inferences from rDNA data. J. Phycol. 41:1039–1054.

Chekanov, K., Fedorenko, T., Kublanovskaya, A., Litvinov, D. & Lobakova, E. 2020. Diversity of carotenogenic microalgae in the White Sea polar region. FEMS Microbiol. Ecol. 96:fiz183.

Chelebieva, E. S., Dantsyuk, N. V., Chekanov, K. A., Chubchikova, I. N., Drobetskaya, I. V., Minyuk, G. S., Lobakova, E. S. & Solovchenko, A. E. 2018. Identification and morphological-physiological characterization of astaxanthin produce strains of *Haematococcus pluvialis* from the Black Sea region. Appl. Biochem Microbiol. 54:639–648.

Damiani, M. C., Leonardi, P. L., Pieroni, O. E. & Cáceres, E. J. 2006. Ultrastructure of the cyst wall of *Haematococ-*

cus pluvialis (Chlorophyceae): wall development and behaviour during cyst germination. Phycologia 45:616–623.

Droop, M. R. 1956. *Haematococcus pluvialis* and its allies. I. The Sphaerellaceae. Rev. Algol. 2:53–71.

Du, F., Hu, C., Sun, X., Zhang, L. & Xu, N. 2021. Transcriptome analysis reveals the promoting effect of trisodium citrate on astaxanthin accumulation in *Haematococcus pluvialis* under high light condition. Aquaculture 543:736978.

Edgar, R. C. 2004. MUSCLE: a multiple sequence alignment method with reduced time and space complexity. BMC Bioinformatics 5:113.

Elliott, A. M. 1934. Morphology and life history of *Haematococcus pluvialis*. Arch. Protistenkd. 82:250–272.

Fang, H., Zhuang, Z., Huang, L., Niu, J. & Zhao, W. 2022. A newly isolated strain of *Haematococcus pluvialis* GXU-A23 improves the growth performance, antioxidant and anti-inflammatory status, metabolic capacity and mid-intestine morphology of juvenile *Litopenaeus vannamei*. Front. Physiol. 13:882091.

Felsenstein, J. 1985. Confidence limits on phylogenies: an approach using the bootstrap. Evolution 39:783–791.

Flot, J. -F., Hespeels, B., Li, X., Noel, B., Arkhipova, I., Danchin, E. G. J., Hejnol, A., Henrissat, B., Koszul, R., Aury, J. -M., Barbe, V., Barthélémy, R. -M., Bast, J., Bazykin, G. A., Chabrol, O., Couloux, A., Da Rocha, M., Da Silva, C., Gladyshev, E., Gouret, P., Hallatschek, O., Hecox-Lea, B., Labadie, K., Lejeune, B., Piskurek, O., Poulain, J., Rodriguez, F., Ryan, J. F., Vakhrusheva, O. A., Wajnberg, E., Wirth, B., Yushenova, I., Kellis, M., Kondrashov, A. S., Welch, D. B. M., Pontarotti, P., Weissenbach, J., Wincker, P., Jaillon, O. & Van Doninck, K. 2013. Genomic evidence for ameiotic evolution in the bdelloid rotifer *Adineta vaga*. Nature 500:453–457.

Gómez, P. I., Haro, P., Lagos, P., Palacios, Y., Torres, J., Sáez, K., Castro, P., González, V., Inostroza, I. & González, M. A. 2016. Intraspecific variability among Chilean strains of the astaxanthin-producing microalga *Haematococcus pluvialis* (Chlorophyta): an opportunity for its genetic improvement by simple selection. J. Appl. Phycol. 28:2115–2122.

González, M. A., Cifuentes, A. S. & Gómez, P. I. 2009. Growth and total carotenoid content in four Chilean strains of *Haematococcus pluvialis* Flotow, under laboratory conditions. Gayana Bot. 66:58–70.

Guo, H., Li, T., Zhao, Y. & Yu, X. 2021. Role of copper in the enhancement of astaxanthin and lipid coaccumulation in *Haematococcus pluvialis* exposed to abiotic stress conditions. Bioresour. Technol. 335:125265.

Harris, E. 2009. *The Chlamydomonas sourcebook. Vol. I. Introduction to Chlamydomonas and its laboratory use*. 2nd ed. Academic Press, Amsterdam, 444 pp.

Hazen, T. E. 1899. The life history of *Sphaerella lacustris* (*Haematococcus pluvialis*). Mem. Torrey Bot. Club 6:211–246.

Herrick, F. H. 1899. On *Haematococcus*. Science 9:319–320.

Karuppan, R., Javee, A., Gopidas, S. K., Pathmanapan, A., Kattusamy, K., Narayanan, V., Subramanian, S. R. & SubramanI, N. 2022. Impact of cultivation parameters on astaxanthin accumulation in the green alga *Haematococcus lacustris* RRGK isolated from Himachal Pradesh, India. Energy Nexus 6:100083.

Kim, B., Lee, S. Y., Narasimhan, A. L., Kim, S. & Oh, Y. -K. 2022. Cell disruption and astaxanthin extraction from *Haematococcus pluvialis*: recent advances. Bioresour. Technol. 343:126124.

Kim, J. H., Affan, A., Jang, J., Kang, M. -H., Ko, A. -R., Jeon, S. -M., Oh, C., Heo, S. -J., Lee, Y. -H., Ju, S. -J. & Kang, D. -H. 2015. Morphological, molecular, and biochemical characterization of astaxanthin-producing green microalga *Haematococcus* sp. KORDI03 (Haematococcaceae, Chlorophyta) isolated from Korea. J. Microbiol. Biotechnol. 25:238–246.

Kim, T. Y., Lee, S. -H. & Lee, S. -Y. 2021. Two newly identified *Haematococcus* strains efficiently accumulated radioactive cesium over higher astaxanthin production. Environ. Res. 199:111301.

Klochkova, T. A., Kwak, M. S., Han, J. W., Motomura, T., Nagasato, C. & Kim, G. H. 2013. Cold-tolerant strain of *Haematococcus pluvialis* (Haematococcaceae, Chlorophyta) from Blomstrandhalvøya (Svalbard). Algae 28:185–192.

Kumar, S., Stecher, G. & Tamura, K. 2016. MEGA7: Molecular Evolutionary Genetics Analysis version 7.0 for bigger datasets. Mol. Biol. Evol. 33:1870–1874.

Lee, Y. -K. & Ding, S. -Y. 1994. Cell cycle and accumulation of astaxanthin in *Haemtaococcus lacustris* (Chlorophyta). J. Phycol. 30:445–449.

Maciver, S. K. 2016. Asexual amoebae escape Muller's ratchet through polyploidy. Trends Parasitol. 32:855–862.

Maddison, W. P. & Maddison, D. R. 2019. Mesquite: a modular system for evolutionary analysis. Version 3.61. Available from: http://www.mesquiteproject.org. Accessed Sep 17, 2022.

Mann Whitney U test calculator, Statistics Kingdom. 2017. Available from: http://www.statskingdom.com/170median_mann_whitney.html. Accessed Sep 17, 2022.

Mazumdar, N., Gopalakrishnan, K. K., Visnovsky, G. & Novis, P. M. 2018. A novel alpine species of *Haematococcus* (Chlamydomonadales: Chlorophyta) from New Zealand. N. Z. J. Bot. 56:216–226.

McCracken, D. A., Nadakavukaren, M. J. & Cain, J. R. 1980. A biochemical and ultrastructural evaluation of the taxonomic position of *Glaucosphaera pplanate* Korsh. New Phytol. 86:39–44.

Mota, G. C. P., de Moraes, L. B. S., Oliveira, C. Y. B., Oliveira, D. W. S., de Abreu, J. L., Dantas, D. M. M. & Gálvez, A. O. 2022. Astaxanthin from *Haematococcus pluvialis*: process, applications, and market. Prep. Biochem. Biotechnol. 52:598–609.

Muller, H. J. 1932. Some genetic aspects of sex. Am. Nat. 66:118–138.

Munakata, H., Nakada, T., Nakahigashi, K., Nozaki, H. & Tomita, M. 2016. Phylogenetic position and molecular chronology of a colonial green flagellate, *Stephanosphaera pluvialis* (Volvocales, Chlorophyceae), among unicellular algae. J. Eukaryot. Microbiol. 63:340–348.

Nakada, T., Misawa, K. & Nozaki, H. 2008. Molecular systematics of Volvocales (Chlorophyceae, Chlorophyta) based on exhaustive 18S rRNA phylogenetic analyses. Mol. Phylogenet. Evol. 48:281–291.

Nakada, T. & Ota, S. 2016. What is the correct name for the type of *Haematococcus* Flot. (Volvocales, Chlorophyceae)? Taxon 65:343–348.

Nozaki, H., Itoh, M., Uchida, H., Watanabe, M. M. & Kuroiwa, T. 1995. Phylogenetic relationships within the colonial Volvocales (Chlorophyta) inferred from *rbc*L gene sequence data. J. Phycol. 31:970–979.

Oslan, S. N. H., Shoparwe, N. F., Yusoff, A. H., Rahim, A. A., Chang, C. S., Tan, J. S., Oslan, S. N., Armugam, K., Ariff, A. B., Sulaiman, A. Z. & Mohamed, M. S. 2021. A review on *Haematococcus pluvialis* bioprocess optimization of green and red stage culture conditions for the production of natural astaxanthin. Biomolecules 11:256.

Peebles, F. 1909. The life history of *Sphaerella lacustris* (*Haematococcus pluvialis*), with especial reference to the nature and behaviour of the zoospores. Zentralblatt Bakteriol. Jena Abt. II 24:511–521.

Pegg, C., Wolf, M., Alanagreh, L., Portman, R. & Buchheim, M. A. 2015. Morphological diversity masks phylogenetic similarity of *Ettlia* and *Haematococcus* (Chlorophyceae). Phycologia 54:385–397.

Pocock, M. A. 1960. *Haematococcus* in southern Africa. Trans. R. Soc. S. Afr. 36:5–55.

Reinicke, D. L., Castillo-Flores, A., Boussiba, S. & Zarka, A. 2018. Polyploid polynuclear consecutive cell-cycle enables large genome-size in *Haematococcus pluvialis*. Algal Res. 33:456–461.

Ringo, D. L. 1967. Flagellar motion and fine structure of the flagellar apparatus in *Chlamydomonas*. J. Cell Biol. 33:543–571.

Rizzo, A., Ross, M. E., Norici, A. & Jesus, B. 2022. A two-step process for improved biomass production and non-destructive astaxanthin and carotenoids accumulation in *Haematococcus pluvialis*. Appl. Sci. 12:1261.

Ronquist, F., Teslenko, M., van der Mark, P., Ayres, D. L., Darling, A., Höhna, S., Larget, B., Liu, L., Suchard, M. A. & Huelsenbeck, J. P. 2012. MrBayes 3.2: efficient Bayesian phylogenetic inference and model choice across a large model space. Syst. Biol. 61:539–542.

Santos, M. F. & Mesquita, J. F. 1984. Ultrastructural study of *Haematococcus lacustris* (Girod.) Rostafinski (Volvocales) I. Some aspects of carotenogenesis. Cytologia 49:215–228.

Schulze, B. 1927. Zur Kentniss einiger Volvocales (*Chlorogonium*, *Haematococcus*, *Stephanosphaera*, Spondylomoraceae und *Chlorobrachis*). Arch. Protistenkd. 58: 508–576.

Shapiro Wilk Test calculator, Statistics Kingdom. 2017. Available from: https://www.statskingdom.com/doc_shapiro_wilk.html. Accessed Sep 17, 2022.

Smith, D. R. 2018. *Haematococcus lacustris*: the makings of a giant-sized chloroplast genome. AoB Plants 10:ply058.

Swofford, D. L. 2003. PAUP*. Phylogenetic analysis using parsimony (*and other methods). Version 4. Sinauer Associates, Sunderland, MA.

Triki, A., Maillard, P. & Gudin, C. 1997. Gametogenesis in *Haematococcus pluvialis* Flotow (Volvocales, Chlorophyta). Phycologia 36:190–194.

Wang, F., Guo, B., Wu, M., Huang, L. & Zhang, C. 2019. A novel strategy for the hyper-production of astaxanthin from the newly isolated microalga *Haematococcus pluvialis* JNU35. Algal Res. 39:101466

Wilcoxon Signed-Ranks test calculator, Statistics Kingdom 2017. Available from: https://www.socscistatistics.com/tests/signedranks/default2.aspx. Accessed Sep 17, 2022.

Yu, C., Wang, H. -P., Qiao, T., Zhao, Y. & Yu, X. 2021. A fed-batch feeding with succinic acid strategy of astaxanthin and lipid hyper-production in *Haematococcus pluvialis*. Bioresour. Technol. 340:125648.